EXCITATION AND FAR FIELD SPECTROSCOPY OF SURFACE PLASMONS IN GOLD NANOSTRUCTURES

An Honors Fellows Thesis

by

SIYING PENG

Submitted to the Honors Programs Office
Texas A&M University
in partial fulfillment of the requirements for the designation as

HONORS UNDERGRADUATE RESEARCH FELLOW

April 2010

Major: Physics and Mathematics

EXCITATION AND FAR FIELD SPECTROSCOPY OF SURFACE PLASMONS IN GOLD NANOSTRUCTURES

An Honors Fellows Thesis

by

SIYING PENG

Submitted to the Honors Programs Office
Texas A&M University
in partial fulfillment of the requirements for the designation as

HONORS UNDERGRADUATE RESEARCH FELLOW

Approved by:

Research Advisor: Alexandre Kolomenski
Associate Director of the Honors Programs Office: Dave A. Louis

April 2010

Major: Physics and Mathematics

ABSTRACT

Excitation and Far Field Spectroscopy of Surface Plasmons in Gold Nanostructures.
(April 2010)

Siying Peng
Department of Physics
Texas A&M University

Research Advisor: Dr. Alexandre Kolomenski
Department of Physics

The properties of surface plasmons (SPs) and their excitation by a light wave are considered. The interaction of light with a metal nanostructure resulted in transmission, reflection and diffraction of light. The spectra of light obtained from these channels display excitation of SP modes at certain incidence angles and wavelengths. The interaction of SP modes near the normal incidence can result in energy and momentum spectral gaps and variations of the widths of SP resonances. The SP dispersion relations were described with the model of two coupled modes, and the spectral amplitude distribution of the transmitted and reflected light were simulated following Rayleigh approach.

DEDICATION

To my father Yong Peng and my mother Yang Xiang.

ACKNOWLEDGMENTS

I thank Alexandre Kolomenski for supervising this work and Hans Schuessler for providing the opportunity to work in his laboratory and his support; John Noel and Winfried Teizer for providing the samples produced with electron beam nanolithography and characterization of these samples; Jeshurun Hembd and Andrei Kolomenski for their numerous contributions to this work and Wonmuk Hwang for providing AFM for sample profile measurements.

I am grateful to my father, mother and grandparents for their encouragement and support. Many thanks to Sandi Smith for her precious help as my undergraduate advisor. I also thank my cousin, Xiaoxian Yin, and Laura E. Martin for their friendship and kindness.

This work was partially supported by the Robert A. Welch Foundation (grant No. A1546), the National Science Foundation (grants Nos. 0722800 and 0555568) and the Air Force Office of Scientific Research (grant FA9550-07-1-0069).

NOMENCLATURE

AM	Air-Metal
AFM	Atomic Force Microscope
ATIR	Attenuated Total Internal Reflection
CCD	Charge Coupled Device
FDTD	Finite Difference Time Domain
SEM	Scanning Electron Microscope
SM	Substrate-Metal
SNOM	Scanning Near Field Optical Microscope
SP	Surface Plasmon
SPP	Surface Plasmon Polariton
SPR	Surface Plasmon Resonance

TABLE OF CONTENTS

Page

ABSTRACT iii

DEDICATION iv

ACKNOWLEDGMENTS v

NOMENCLATURE vi

TABLE OF CONTENTS vii

LIST OF FIGURES viii

LIST OF TABLES ix

CHAPTER

I INTRODUCTION AND LITERATURE REVIEW 1

A. Early studies 1
B. Later developments 2
C. Light interaction with gratings 2
D. Theoretical approaches 3
E. Some recent trends in the study of the interaction of light with periodic metal structures 4
F. Formulation of the research aim 6

II PROPERTIES OF SURFACE PLASMONS IN METALLIC STRUCTURES 7

A. Derivation of the dispersion equation for a planar geometry 7
B. SP excitation due to interaction with a grating 14
C. Propagation length of surface plasmons 17

III STUDY OF SURFACE PLASMON MODES IN METAL NANOSTRUCTURES WITH THE FAR FIELD SPECTROSCOPY 26

A. Investigated samples 26
B. Transmission for front-illuminated samples 27

CHAPTER Page

C. Transmission for back-illuminated samples 30
D. Reflection from front-illuminated samples 31
E. Reflection from back-illuminated samples 33
F. Diffraction 34
G. Reflection, transmission and diffraction in the interaction of light with a grating 36

IV BAND GAPS OF SP MODES IN METAL NANOSTRUCTURES 40

A. Previous studies 40
B. Experimental investigation of laser light interaction with gold nanostructures 40
C. Interpretation of avoided crossing and spectral gaps with coupled mode theory 45
D. Calculation of the dispersion relations of SPs modes and comparisons to experiment 47

V SUMMARY AND CONCLUSIONS 50

REFERENCES 51

APPENDIX A 55

APPENDIX B 57

CONTACT INFORMATION 59

LIST OF FIGURES

FIGURE Page

1 Schematic representation of the excitation of a SP and its scattering on the surface roughness 14

2 Frequency and wave-number diagram calculated with Mathematica 16

3 Angle-wavelength dependence of $\pm 1^{st}$ order diffraction cutoff 18

4 Measured and calculated SPR curves for (a) 633 nm and (b) 805 nm 22

5 Attenuation lengths for (a) gold and (b) silver, calculated for a broad spectral range with the exact (solid lines and solid lines with triangles) and approximate (dashed lines) models 24

6 The influence of the thickness of the gold film on the properties of SPs: SP resonance curves at 633 nm for different film thicknesses 25

7 A portion of the SEM data for Sample 2 (cross section and measurements from the blue line in the image) 26

8 Dependence of the normalized transmission on the wavelength versus incidence angle from 0 to 5 degrees. (Sample 2) 28

9 Wavelength versus incidence angle for the transmission minimum. (Sample 2) 29

10 Angular dependences of the coupling for the -1 order and +1 order SP modes in transmission. (Sample 2) 29

11 Wavelength versus angle for minima in transmission from back illuminated sample (Sample 1) 30

12 Angular dependence of the coupling in transmission for back illuminated sample. (Sample 1) 31

13 Dependence of the normalized reflection on the wavelength for incidence angles from 0 to 3 degrees. (Sample 2) 32

FIGURE Page

14 Wavelength versus incidence angle for the reflection minimum (Sample 2) 33

15 Reflection and transmission spectra ((a) Sample 1, (b) Sample 2)……...33

16 Diffraction spectra versus wavelength of a front illuminated sample at incidence angle of 2.5 degrees (Sample 1).....35

17 Dependence of coupling on the polarization angle, with 0 degrees corresponding to polarization in the plane of incidence.....36

18 Calculation of transmission spectra for wavelength versus incidence angle from -1 to 1 degrees: period=705 nm, wire width=350 nm 39

19 Measured samples: (a). Schematic of the sample profile and the geometry of the laser beam incidence (red arrows).....41

20 Transmitted light intensity for different incidence angles and wavelengths: (a,b) sample 1A, (c,d) sample 2A.....43

21 Observed and calculated SP modes in the avoided crossing region: (a, d) minima of the transmission from the experiment, (b,e) transmitted intensity vs. angle for a set of wavelengths and (c,f) calculation of the SP modes of $n = \pm 1$ orders taking into account their interaction (Eq. (3), details in the text).....45

LIST OF TABLES

TABLE Page

1. Dielectric constants of gold ε_1 and glass ε_2; SP attenuation length without roughness L_{sp}; effective dielectric constant $\varepsilon_{1,eff}$; attenuation length $L_{sp,r}$ calculated with roughness ($\delta = 2.0\,\text{nm},\ \sigma = 36\,\text{nm}$) and experimentally determined SP attenuation lengths 23

CHAPTER I

INTRODUCTION AND LITERATURE REVIEW

A. Early studies

In 1902, it was discovered by Robert Wood [1] that when light is incident on a metallic grating abrupt variations of the intensity of the reflected light take place at certain wavelengths. This phenomenon is known in the literature as Wood's anomalies, and Rayleigh was the first who tried to explain it theoretically [2]. Rayleigh's theory indeed provided an explanation to some of these anomalies that are related to passing over the horizon of waves, corresponding to certain diffraction orders; however, other anomalies as was shown by Fano [3], resulted from the interaction of light with surface waves. It should be noted that Sommerfeld and Zenike independently discovered the existence of surface electromagnetic waves using theoretical approach [4-5]. However, only later Fano was the first to relate certain class of Wood anomalies with such surface waves [3].

In a paper by Ritchie *et al* [6] some Wood's anomalies are explained as the result of the excitation of SPs on the metal surface due to special properties of the diffraction on metallic gratings. They produced gratings of Al and Au, and have also obtained clear evidence for frequency gaps in the dispersion curves for surface plasmons. More recently, there was considerable interest in studies of the interaction of light with

---

This thesis follows the style of Physical Review B.

metallic structures [7-12], since such structures can couple and guide light.

B. Later developments

Since the works of Kretchmann and Raether [13], the Attenuated Total Internal Reflection (ATIR) geometry, employing the matching of the propagation velocities of the incident light and SPs along the metal surface (SP resonance condition), was one of the most commonly used. Several new directions emerged more recently. The sensitivity of the propagation velocity of SPs to dielectric properties of the adjacent medium makes them an efficient tool in biosensing [14]. The attenuation of SPs determines the width of the SP resonance, which affects the sensitivity of the sensor [15]. The propagation length of SPs determines also the spatial resolution in imaging technique with the ATIR geometry [16]. Planar optical geometry is attractive for compact optical devices interconnected with electronic components, therefore the development of optics of SPs [17] is also one of the promising directions of research. It was shown that for a symmetrical structure of a metal film, sandwiched between two dielectric layers a mode of long-range SPs can propagate [18].

C. Light interaction with gratings

The interaction of light with periodic metal structures, allowing for efficient coupling of light to surface plasmons (SPs) with their remarkable properties, such as sharp

resonances [1,2,6,19], localization and enhancement of the electromagnetic field [20,21], and wave guiding along metal surfaces [22] continues attracting considerable interest. In particular, mimicking SPs by metal nanostructures with holes [23] and enhancing light absorption [24,25] were demonstrated. Recently, after the discovery of the extraordinary light transmission through arrays of small holes [26] the investigation of the role of SPs in this phenomenon demonstrated that the transmission minima correspond to the excitation of the SP modes [27].

The interaction of light with periodic structures is also of interest, because excited SPs exhibit gaps in the energy spectrum (ω-gaps) [6,17,20,21], rendering these structures as simple plasmonic crystals. The gaps appear due to mode interaction near the crossing of their unperturbed dispersion curves. The existence of momentum gaps (or k-gaps) was also discovered in experiments [28].

D. Theoretical approaches

There are various ways to calculate the transmission and reflection coefficient of light incident on a metallic grating. The general Scattering Matrix Method was proposed by Whittaker and Culshaw [29]. Tikhodeev et al. applied it to photonic crystal slabs [30] by representing the system as a set of thin layers and considering the solution of Maxwell Equations in each layer. Transfer Matrix formalism was used to combine the input and output field vectors from adjacent layers. The Finite Difference Time Domain (FDTD) method is used for calculations of electromagnetic wave interaction with material

structures. The basic FDTD grid and time-stepping algorithm is first developed by Kane Yee [31]. In this approach, the solution of Maxwell equations in each Yee lattice is considered in time domain and multiple dimensions can be considered. Botten et al. developed a rigorous theory describing the diffraction for both dielectric and highly conducting gratings [32-34]. They solved the Helmholtz equation within the grating region to obtain a transcendental equation for eigen values. The field in the grating was presented as a linear combination of the eigen-functions, satisfying boundary conditions at the grating. The field outside the grating was described as a Rayleigh sum of different diffraction orders. By matching the boundary conditions of electric and magnetic fields at the interface, the transmission and reflection coefficients are obtained. Lochbihler did a reasonable approximation which simplifies Botten's model by ignoring the field in the wires and using constant impedance [35].

E. Some recent trends in the study of the interaction of light with periodic metal structures

Instead of using a one dimensional periodic structure, Altewischer et al. [36] investigate excitation and propagation of SPs in a metallic structure with a two dimensional structure. With a hexagonal nanohole array, they used microscopic imaging and observed forking of the propagation SP beams. It is concluded that forking is due to Bragg reflection. In the transmission spectrum, they observe wings besides the central transmission peak, which was considered due to the resonant excitation of SPs that propagate on the array.

Pendry et. al. [23] proposed designer Surface Plasmons. Surface plasmon modes don't exist in highly conducting metal due to small internal losses. By perforating holes in the surface of highly conducting surface plasmon modes can exist. He suggested that by controlling the size and spacing of the perforated holes, designer surface plasmons can be created with any dispersion relation.

Bozhevolnyi et al. [37] study a structure with metal spots on gold film arranged in periodic triangular lattice. The experimental set up consists of a Scanning Near Field Optical Microscope (SNOM) and an arrangement for the SPPs excitation in the Kretschmann configuration. They consider the internal damping as the limit of the propagation length of SPP's. They observed a strong difference of intensity distributions inside and outside of the structures, which diminishes at longer wavelength.

Christ et al. studied the coupling between localized and delocalized surface plasmon modes by a multilayer metallic crystal slab, representing a photonic crystral [38]. The system they studied was one-dimensional gold nanowire array on top of the SiO2 spacer layer with underlying 20-nm-thick homogeneous silver film. They observed one minimum in transmission spectra without the silver film. With the system consist of the silver film, they observe two minima while the resonance at longer wavelength is broader and deeper. They consider the two minima in the spectrum as a localized magnetic plasmon mode and a grating-induced excitation of an extended surface

plasmon mode. The coupling of localized and delocalized modes leads to an enhanced resonant absorption for structures with intermediate spacer layer thicknesses.

Vasa et al. observe SPP-quantum well interaction [39]. They studied experimentally a 80nm thick gold grating with period 500nm deposited on top of a semiconductor. SPP excitation at both air-metal and substrate-metal interfaces was observed. They studied the reflection from the sample, where the coupling among the modes AM [-1], SM [+2], SM [-3] is dominating.

F. Formulation of the research aim

In the present work we study experimentally the interaction of light with SPs on a gold grating through transmission, reflection and diffraction. For the theoretical description of this interaction we follow a general approach proposed by Rayleigh and developed by Botten et al. [33-34] and Lochbihler [35]. Considering interaction of SP modes and formation of spectral gaps, we use the model of two coupled modes.

CHAPTER II

PROPERTIES OF SURFACE PLASMONS IN METALLIC STRUCTURES

A. Derivation of the dispersion equation for a planar geometry

A special type of an electromagnetic wave can exist, which is localized near the surface. This propagating mode of oscillations, decaying exponentially on both sides of the interface of two adjacent media is referred to as surface wave.

Difference types of surface waves can exist in nature. Along surfaces of solids can propagate surface acoustic waves, discovered at the beginning of the 20th century by Rayleigh. This wave propagate along the Earth surface, when, for instance, earthquakes happen. Surface electromagnetic waves were first studied theoretically by Sommerfeld [4] and Zenneck [5]. However, their relation with the electronic oscillations (plasmons) and a subsequent extensive study started in the middle of the 20th century, and these waves received the name “surface plasmon polaritons” or simply “surface plasmons”.

We assume a system comprised of a metal half-space bordering with a dielectric and that there are no external charges and currents in the system and the magnetic susceptibility is 1. Then for electromagnetic field in this system we have a set of Maxwell’s equations:

$$\nabla \times \vec{H} = \varepsilon \frac{1}{c} \frac{\partial \vec{E}}{\partial t} \tag{1}$$

$$\nabla \times \vec{E} = -\frac{1}{c}\frac{\partial \vec{H}}{\partial t} \tag{2}$$

$$\nabla \cdot \varepsilon \vec{E} = 0 \tag{3}$$

$$\nabla \cdot \vec{H} = 0 \tag{4}$$

We consider a reference frame with x-axis along the interface and y-axis perpendicular to the interface. Then by applying Maxwell's equations to every medium and using the requirements of the continuity at the interface we obtain the boundary conditions:

$$E_{1x} = E_{2x} \tag{5}$$

$$H_{1y} = H_{2y} \tag{6}$$

$$\varepsilon_1 E_{1z} = \varepsilon_2 E_{2z} \tag{7}$$

For derivation of boundary conditions (5,6,7) see Appendix A.

From (1) and (2) it follows that electric and magnetic fields satisfy the wave equation. Indeed if we apply curl to both sides of equations (1) and (2) then we get:

$$\nabla \times (\nabla \times \vec{H}) = \nabla(\nabla \cdot \vec{H}) - \nabla^2 \vec{H} = -\nabla^2 \vec{H}$$

The right hand side:

$$\frac{\varepsilon}{c}\frac{\partial}{\partial t}(\nabla \times \vec{E}) = \frac{\varepsilon}{c}\frac{\partial}{\partial t}(-\frac{1}{c}\frac{\partial}{\partial t}\vec{H}) = -\frac{\varepsilon}{c^2}\frac{\partial^2 \vec{H}}{\partial t^2}$$

Thus,

$$\nabla^2 \vec{H} - \frac{\varepsilon}{c^2}\frac{\partial^2 \vec{H}}{\partial t^2} = 0 \tag{8}$$

Similarly, we obtain the relation for electric field by applying curl to eq. (2):

$$\nabla^2 \vec{E} - \frac{\varepsilon}{c^2}\frac{\partial^2 \vec{E}}{\partial t^2} = 0 \tag{9}$$

The Eqs. (8,9) are wave equations since they describe propagating of electromagnetic waves.

Particular solutions of the Eqs.(8,9) are plane electromagnetic waves. Indeed, let us seek the solutions of the form (it is easy to show that these expressions satisfy of the wave equations (8,9)):

$$\vec{H} = \vec{H}_0 \, Exp[i(\vec{k}\cdot\vec{r} - \omega t)] \tag{10}$$

$$\vec{E} = \vec{E}_0 \, Exp[i(\vec{k}\cdot\vec{r} - \omega t)] \tag{11}$$

where $\vec{k}$ is the wave vector and ω is frequency of the wave. Then immediately, from Eqs. (1,2) we see that the electric field and magnetic field are perpendicular to each other and perpendicular to the wave vector and, this means, to the propagation direction.

Indeed,

$\nabla \times \vec{H} = i\vec{k} \times \vec{H}$ is parallel to $\vec{E}$ from (1)

$\nabla \times \vec{E} = i\vec{k} \cdot \vec{E}$ is parallel to $\vec{H}$ from (2)

$\vec{k} \cdot \vec{E} = 0$ from (3)

$\vec{k} \cdot \vec{H} = 0$ from (4)

Next, we are going to find solutions for the SPs. It is known from the theory of bulk plasmons that they represent a longitudinal mode of electromagnetic oscillations in which electric field is parallel to the propagation direction of the wave.

Thus, we can expect that SPs also have a component of the electric field which is parallel to the propagation direction. On the other hand, they should satisfy the wave equations (8,9) and we can seek the solution in the form of plane waves.

Thus, we seek the solutions of the form:

Medium 1, z<0, in which:

$$k_{1x}{}^2 + k_{1z}{}^2 = \frac{\omega^2}{c_1{}^2} \tag{12A}$$

$$c_1{}^2 = \frac{c^2}{\varepsilon_1^2}$$

$$\vec{H}_1 = (0, H_{1y}, 0) Exp[i(k_{1x}x + k_{1z}z - \omega t)]$$

$$\vec{E}_1 = (E_{1x}, 0, E_{1z}) Exp[i(k_{1x}x + k_{1z}z - \omega t)]$$

Medium 2, z>0

$$k_{2x}{}^2 + k_{2z}{}^2 = \frac{\omega^2}{c_2{}^2} \tag{12B}$$

$$c_2{}^2 = \frac{c^2}{\varepsilon_2^2}$$

$$\vec{H}_2 = (0, H_{2y}, 0) Exp[i(k_{2x}x + k_{2z}z - \omega t)]$$

$$\vec{E}_2 = (E_{2x}, 0, E_{2z}) Exp[i(k_{2x}x + k_{2z}z - \omega t)]$$

Substituting these representations into (1) we obtain:

$$\nabla \times \vec{H} = \begin{vmatrix} \hat{x} & \hat{y} & \hat{z} \\ \frac{\partial}{\partial x} & \frac{\partial}{\partial y} & \frac{\partial}{\partial z} \\ H_x & H_y & H_z \end{vmatrix} = -\hat{x}\frac{\partial}{\partial z}H_y + \hat{z}\frac{\partial}{\partial x}H_y$$

Thus, we conclude from (1):

$$\frac{\partial H_{iy}}{\partial z} = -\varepsilon_i \frac{1}{c}\frac{\partial}{\partial t}E_{ix}$$

so that

$$k_{1z}H_{1y} = \frac{\omega}{c}\varepsilon_1 E_{1x}$$

$$k_{2z}H_{2y} = \frac{\omega}{c}\varepsilon_2 E_{2x}$$

Using now eq. (5), we obtain:

$$E_{1x} = \frac{k_{1z}c}{\omega\varepsilon_1}H_{1y} = E_{2x} = \frac{k_{2z}c}{\omega\varepsilon_2}H_{2y}$$

which implies:

$$\frac{k_{1z}}{\varepsilon_1}H_{1y} - \frac{k_{2z}}{\varepsilon_2}H_{2y} = 0$$

In addition we have eq. (6):

$$H_{1y} - H_{2y} = 0$$

The system of algebraic homogeneous equations:

$$\begin{aligned} H_{1y} - H_{2y} &= 0 \\ \frac{k_{1z}}{\varepsilon_1} H_{1y} - \frac{k_{2z}}{\varepsilon_2} H_{2y} &= 0 \end{aligned} \tag{13}$$

has solution which is not trivial only if the determinant D_0 is zero:

$$D_0 = \begin{vmatrix} 1 & -1 \\ \frac{k_{1z}}{\varepsilon_1} & -\frac{k_{2z}}{\varepsilon_2} \end{vmatrix} = \frac{k_{1z}}{\varepsilon_1} - \frac{k_{2z}}{\varepsilon_2} = 0 \tag{14}$$

This last equation represents the dispersion equation for SPs.

We can rewrite it in a more convenient form:

$$\varepsilon_1^2 \left(\frac{\omega^2}{c^2}\varepsilon_2 - k^2\right) = \varepsilon_2^2 \left(\frac{\omega^2}{c^2}\varepsilon_1 - k^2\right)$$

where we introduced wave number $k = k_x$, since surface plasmons propagate along the surface and use the property of plane waves that

$k_x^2 + k_z^2 = \frac{\omega^2}{c_i^2}\varepsilon_i$ (see eq. (12A,B))

Consequently, we get the dispersion equation:

$$k^2 = \frac{\omega^2}{c^2}\frac{\varepsilon_1 \varepsilon_2}{\varepsilon_1 + \varepsilon_2} \tag{15}$$

We would like to have a solution which localized to the surface, i.e. it decays with distance from the interface on both sides.

Thus, we want to have k_{1z} and k_{2z} imaginary to provide conditions:

$Exp[ik_{1z}z] \xrightarrow{z \to -\infty} 0$

$Exp[ik_{2z}z] \xrightarrow{z \to +\infty} 0$

Consequently,

for q1 and q2 as real numbers, we let:

$$k_{1z} = \sqrt{\frac{\omega^2}{c^2}\varepsilon_2 - k^2} = -iq_1, \qquad q_1 > 0$$

$$k_{2z} = \sqrt{\frac{\omega^2}{c^2}\varepsilon_1 - k^2} = iq_2, \qquad q_2 > 0$$

Then our initial dispersion equation (14) becomes:

$\frac{q_1}{\varepsilon_1} + \frac{q_2}{\varepsilon_2} = 0$, where $q_{1,2} > 0$

We see that this condition can be fulfilled only when ε_1 or ε_2 are negative.

Since we are looking for propagating surface waves, the wavenumber should be real and

$$k^2 = \frac{\omega^2}{c^2}\frac{\varepsilon_1\varepsilon_2}{\varepsilon_1 + \varepsilon_2} > 0.$$

Suppose that ε_2 corresponds to a dielectric and $\varepsilon_2 > 0$, then the above inequality is possible only if

$$\varepsilon_1 < -\varepsilon_2 \tag{16}$$

Thus, we obtained the condition when the existence of SPs is possible.

Now we need to understand for which materials this condition can be fulfilled.

By using the Drude model for the dielectric properties, it is easy to show that this is possible in a metal and also in a doped semiconductor at the frequencies below the frequency of bulk plasmonic oscillations.

According to Drude's model (see Appendix B) the dielectric function of a free electron gas is $\varepsilon = 1 - \frac{\omega_P^2}{\omega^2}$, where $\omega_P = \sqrt{4\pi e N \frac{e^2}{m}}$ is the so called plasmon frequency.

Thus we can see that in some interval of optical frequencies, when $\omega < \omega_P$, the dielectric constant is negative and its absolute values increases with decreasing frequency, and therefore

$$\varepsilon = \frac{D}{E} = \frac{E + P}{E} = 1 - 4\pi e N \frac{eE_0}{m\omega^2} \tag{17}$$

can be satisfied and, consequently, the existence of SPs is possible.

B. SP excitation due to interaction with a grating

Although the excitation of SPs with a prism is quite common [13], in this work we will consider their excitation via an interaction with a grating. Fig. 1 shows schematically the interaction of light with a grating. SPs are in the plane of a metal film, and the bulk light wave is incident at an angle with the metal film.

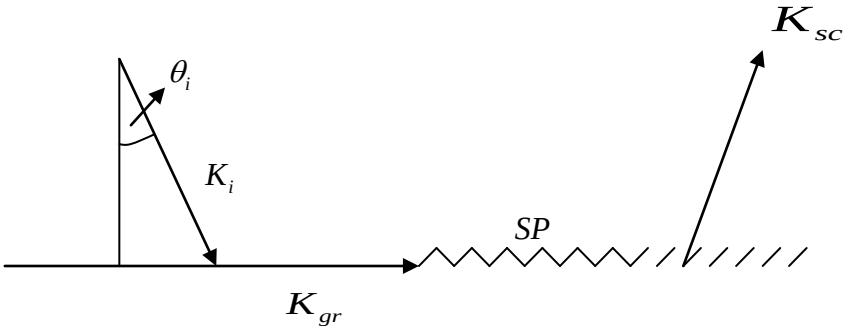

Fig. 1. Schematic representation of the excitation of a SP and its scattering on the surface roughness.

Coupling happens when the wave vector of the light after its interaction with the grating has a component in the plane of the grating equal to the wave vector of the surface plasmon.

$$\boldsymbol{K}_i \sin\boldsymbol{\theta}_i + \boldsymbol{K}_{gr} = \boldsymbol{K}_{sp}$$
$$\boldsymbol{K}_{sp} - \boldsymbol{K}_{gr} = \boldsymbol{K}_{sc} \sin\boldsymbol{\theta}_{sc}$$

The second equation describes the scattering of a SP on the grating.

Preliminary calculations were performed for a 3-layer system consisting of air (ε_1), silver (ε_m) and silicon (ε_2) interacting with light incident at angle θ. We calculated the resonance angle for the SP mode excitation from the condition $K = K_p + \Delta K_p = K_x$, in which K is a function of ω. The resonance angle can be found in the $\omega - K$ diagram (see Fig. 2) from the intersection of the straight line $K_x = \frac{n\sin\theta}{c}\omega + K_g$ with the dispersion curve of SP. The refractive index of SP is $n_p = \sqrt{\frac{\varepsilon_1 \cdot \varepsilon_m}{\varepsilon_1 + \varepsilon_m}}$, the wave number of SP is $K_p = \frac{\omega \cdot n_p}{c}$, and the correction of wave number is $\Delta K_p = \frac{a^2 - {\varepsilon_1}^2}{a^2 + {\varepsilon_1}^2} \cdot g$, in which $a = |\varepsilon_m| \cdot (\varepsilon_1 - \varepsilon_2) - \varepsilon_1 \cdot \varepsilon_2$, $g = 2 \cdot K_p \cdot {n_p}^2 \cdot \exp[-2 \cdot K_p \cdot \sqrt{\frac{\varepsilon_m}{\varepsilon_2}} \cdot d_1]$ and d1 is the thickness of the metal film. A correction factor K_{corr} =1.14 was introduced with ω because there is certain deviation from the experimental result.

The alternative way is to calculate for reflection at the interface of the glass and metal film for a three-layer system consisting of glass, gold film and air. The relationship of incident light, grating and SPs is given as follows: $K_i \sin\theta \pm NK_{gr} = K_{sp}$,

in which N is the order of the SP excitation, K_i and θ_i are the wavenumber and incidence angle of the incident light, K_{gr} is the grating constant, and K_{sp} is the wave number of the excited SPs.

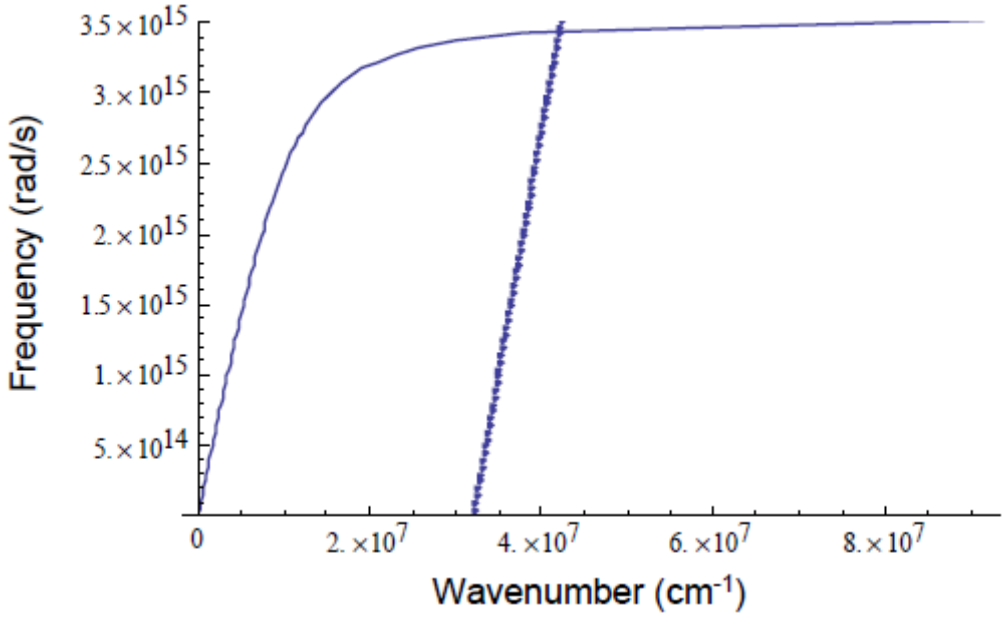

Fig. 2. Frequency and wave-number diagram calculated with Mathematica.

By calculating the angular dependence of the reflection coefficient for light of a given wavelength, we can find the resonance angle which gives minimum reflection of the corresponding wavelength.

$$\sqrt{\varepsilon_{glass}} K \sin\theta_r = K_{sp}$$

In which K is the wave number of incidence light, and θ_r is resonance angle. Combining these two equations, we obtain:

$$\sqrt{\varepsilon_{glass}} K \sin\theta_r = K \sin\theta_i \pm NK_{gr}$$

$$\theta_i = \sin^{-1}[\sqrt{\varepsilon_{glass}} \sin\theta_r \pm \frac{K_{gr}}{K}].$$

The dependence of cutoff wavelength with incidence angles of diffraction orders is given by the equation (See Fig.3 for cutoff wavelength versus incidence angle):

+1 order: $K \sin\theta + K_g = K_{sp}$, $\lambda_{cutoff} = d(1 - \sin\theta)$

-1 order: $K \sin\theta + K_g = K_{sp}$, $\lambda_{cutoff} = d(1 + \sin\theta)$

C. Propagation length of surface plasmons

We directly observed the propagation of SPs supported by a gold film by detecting the scattered light in the far field with a microscope and an attached CCD camera [40]. The experimental results are compared with model calculations on the basis of an exact model and the model derived in the approximation of a relatively thick film and small losses. The relative role of different factors on the attenuation of surface plasmons is

analyzed. The calculations were performed in a broad wavelength interval, while the experimental study was performed at two optical wavelengths for 633 nm and 805 nm.

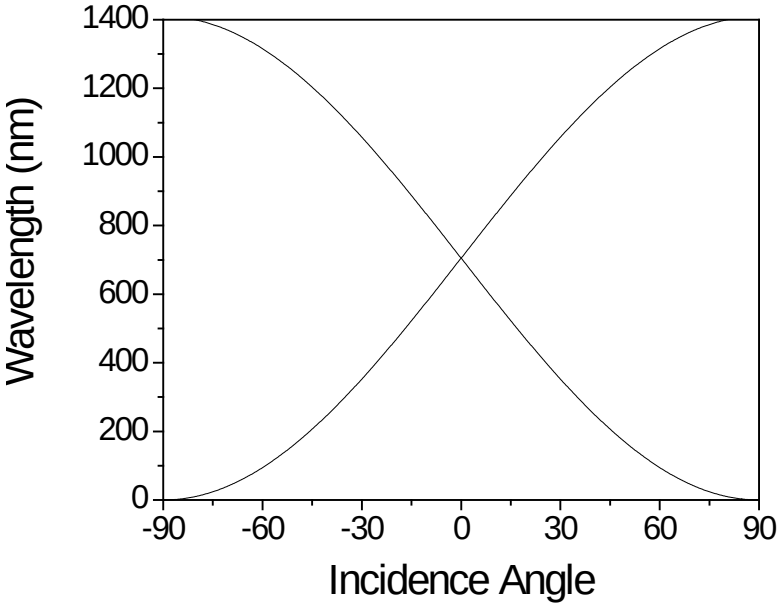

Fig. 3. Angle-wavelength dependence of $\pm 1^{st}$ order diffraction cutoff.

We show [40] that the SP propagation length depends, besides internal and radiational losses, also on the surface roughness. In the approximation and $\varepsilon_{2,r} >> \varepsilon_{2,i}$, which is usually fulfilled for gold and silver films in the optical and IR spectral regions, the reflectivity can be expressed [41] in a Lorentzian form:

$$R = 1 - \frac{4(\Gamma_i + \Gamma_r)\Gamma_{\text{rad}}}{(k - k_{SP,r})(k - k_{SP,r}^*)}, \tag{18}$$

where

$$k_{SP,r} = k_{SP} + (\Delta k_r + i\Gamma_r) = k_p + \Delta k_p + \Delta k_r + i(\Gamma_i + \Gamma_{\text{rad}} + \Gamma_r) \tag{19}$$

is the complex wave number of the SP that takes into account roughness, the star (*) denotes complex conjugation, $\Gamma_i = \Gamma_{i1} + \Gamma_{i2r}$, $k_p = (2\pi n_p / \lambda_0)$ is the wave number of the SP corresponding to the case of infinitely thick metal film and $\Delta k_p = [(a^2 - \varepsilon_0{}^2)/(a^2 + \varepsilon_0{}^2)]g$ is the correction to this number accounting for the finite thickness of the film. The following notations were introduced in the above formulas

$$g = 2k_p n_p{}^2 \exp[-2k_p(\varepsilon_{1r}/\varepsilon_{2r})^{1/2} d_1]/(\mathrm{Re}\,\varepsilon_{2r} + |\varepsilon_{1r}|) \quad , \quad a = |\varepsilon_{1r}|(\varepsilon_0 - \varepsilon_{2r}) - \varepsilon_0\varepsilon_{2r} \quad ,$$

$$n_p = [\varepsilon_{1r}\varepsilon_{2r}/(\varepsilon_{1r} + \varepsilon_{2r})]^{1/2}, \ \Gamma_{i1} = k_p(\varepsilon_{1i}/2\varepsilon_{1r}{}^2)n_p{}^2, \ \Gamma_{i2} = k_p(\varepsilon_{2i}/2\varepsilon_{2r}{}^2)n_p{}^2, \qquad (20)$$

$\Gamma_{\mathrm{rad}} = [2a\varepsilon_0/(a^2 + \varepsilon_0{}^2)]g$. The quantities Γ_{i1} and Γ_{i2} describe the damping that originates from the internal losses in the metal and the adjacent medium respectively and Γ_{rad} describes the radiative loss due to the transmission of light through the metal film. Quantities Δk_r and Γ_r in Eq. (19) describe the changes of the real and imaginary part of the wave number due to surface roughness. The term Γ_r includes contributions to additional attenuation of SPs related to the changes of the dielectric properties owing to the surface roughness, re-scattering losses as well as the losses resulting from the conversion of SPs into radiative bulk waves.

Equation (18) shows explicitly the resonance character of the SP excitation phenomenon, and the resonance is the most pronounced for the optimal metal film thickness $d_{1,opt}$, which is about 47 nm for gold. The inverse of the imaginary part of

$k_{SP,r}$ determines the attenuation length (at e^{-1} level) of the SPs in terms of the SP field amplitude. However, in most experiments what is measured is the decay of the SP intensity, which is proportional to the square of the field. As a result, for the intensity attenuation length a factor of 0.5 must be introduced

$$L_{sp,r} = 0.5\,(\Gamma_{i1} + \Gamma_{i2} + \Gamma_r + \Gamma_{rad})^{-1}. \tag{21}$$

As it follows from Eq. (18), this length can be also approximately determined from the FWHM width $\Delta\theta$ of the resonance curve

$$L_{sp} \approx (\sqrt{\varepsilon_0}\, k_0 \cos\theta_{\text{res}} \Delta\theta)^{-1} \quad . \tag{22}$$

The incident light with a power P_0 scatters from a rough surface on the back side of the metal film yielding the power dP that goes into a of solid angle element $d\Omega$ [42]:

$$dP = 4P_0 \left(\frac{\pi}{\lambda}\right)^4 \frac{|\varepsilon_2|^{0.5}}{\cos\theta} |t_{012}(\theta)|^2 |W(\theta)|^2 \tilde{G}(\mathbf{k}'-\mathbf{k}) d\Omega \,, \tag{23}$$

where θ_0 is the incidence angle of the excitation light, $|t_{012}(\theta)|^2$ is the transmission function for a two-boundary system with a metal film (namely, this function is the square of the ratio of strengths of the magnetic field at the second boundary metal-air and in the incident wave), $|W(\theta)|^2$ is the dipole radiation function of the surface (for an explicit expression see Ref. [17], Eq.(2)); $\tilde{G}(\mathbf{k})$ is the power spectral density (PSD) function

$$\tilde{G}(\mathbf{k}) = \frac{1}{(2\pi)^2}\int G(\mathbf{r})\exp(-i\mathbf{kr})d\mathbf{r} \tag{24}$$

of the correlation function of the surface roughness $\varsigma(\mathbf{r})$:

$$G(\mathbf{r}) = \frac{1}{(2\pi)^2 S}\int_S \varsigma(\mathbf{r}')\varsigma(\mathbf{r}'+\mathbf{r})d\mathbf{r}', \tag{25}$$

where the integral is taken over the illuminated area of the rough surface *S*. In Eq. (23) the argument of the PSD function is the difference of the interface components of the wave vectors of the scattered and incident light. The roughness correlation function is often approximated by a Gaussian function

$$G(\mathbf{r}) = \delta^2 \exp\left(-\frac{r^2}{\sigma^2}\right). \tag{26}$$

where σ is the correlation length and δ is the average height of the roughness. For a one-dimensional PSD function of the surface roughness we obtain

$$\tilde{G}(k_x) = \frac{1}{(2\pi)}\int G(x, y=0)\exp(-ik_x x)dx = \frac{\delta^2\sigma}{2\sqrt{\pi}}\exp\left(-\frac{k_x^2\sigma^2}{4}\right). \tag{27}$$

The roughness changes the complex wavenumber of SPs [43-46], which means also a correction to the SP dispersion equation. We calculated this change due to roughness,

$$\Delta k_{SP} = k_{SP,r} - k_{SP} = \Delta k_r + i\Gamma_r, \tag{28}$$

using Eq. (A42) of Ref. [46]. The real part of Δk is responsible for the angular displacement of the SPR resonance and the imaginary part determines the change in attenuation of SPs and also the change of the width of the resonance curve due to

roughness. Using the approximation of Eqs. (19-20), one can also calculate an *effective dielectric constant* of the metal $\varepsilon_{1,eff}$ that gives the same change Δk_{SP} as the surface roughness (assuming that its contribution is relatively small), i.e. $\varepsilon_{1,eff}$ can be found from the equation

$$[k_p + \Delta k_p + i(\Gamma_i + \Gamma_{\text{rad}})]|_{\varepsilon_1=\varepsilon_{1,eff}} = [k_p + \Delta k_p + \Delta k_r + i(\Gamma_i + \Gamma_r + \Gamma_{\text{rad}})]|_{\varepsilon_1=\varepsilon_1} . \quad (29)$$

The obtained value of $\varepsilon_{1,eff}$ can then be used to calculate the modified by roughness SPR curve, using the approximate expressions of Eqs.(18-20).

The results of the calculations with and without surface roughness are presented in Fig. 4. The curves without roughness were calculated with exact expressions for the three-layer system [41], and the approximate model of Eqs. (18-20) gives close results.

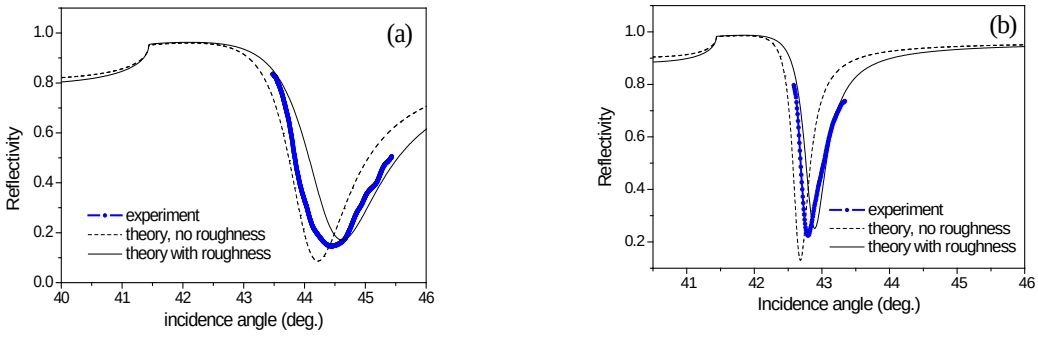

Fig. 4. Measured and calculated SPR curves for (a) 633 nm and (b) 805 nm.

The angular distribution of the reflected light intensity in the vicinity of the SPR angle for 633 nm and 805 nm is shown in Fig. 4. The minima indicate the angular positions of the SP resonance, which occurred at the light incidence angle onto the gold film

interface at 44.5º for 633 nm and at 42.8º for 805 nm. The dashed lines show calculated SPR curves without surface roughness. Thin solid curves are obtained taking into account roughness correction (Eq. (28)), then calculating the value of the effective dielectric constant $\varepsilon_{1,eff}$ by solving Eq. (29). For the calculations we used the dielectric constants compiled in Table 1. The roughness

Table 1. Dielectric constants of gold ε_1 and glass ε_2 ; SP attenuation length without roughness L_{sp}; effective dielectric constant $\varepsilon_{1,eff}$; attenuation length $L_{sp,r}$ calculated with roughness ($\delta = 2.0$ nm, $\sigma = 36$ nm) and experimentally determined SP attenuation lengths.

λ (nm)	ε_1	ε_2	L_{sp} (μm)	$\varepsilon_{1,eff}$	$L_{sp,r}$ (m)	L_{sp} (μm) experiment
633	-10.8+0.76i [47]	2.30	4.4	-9.6+0.62i	3.6	3.0 (Fig. 4(a))
	-11.0+1.5i [48]		3.7	-8.6+0.88i	2.5	
	-9.1+1.0i [49]		2.7	-8.2+0.85i	2.3	
805	-23.0+0.75i [47]	2.28	23	-20.1+0.60i	17	17 (Fig. 4(a))
	-22.3+2.0i [48]		14	-19.6+1.7i	11	
	-26.8+1.8i [49]		24	-22.6+1.3i	18	

parameters were determined from measurements with an AFM. From the profile measurements the 1-D PSD function of the surface roughness was calculated. By fitting the PSD function with a Gaussian of the form of Eq. (27), we determined $\delta = 2.0$ nm and $\sigma = 36$ nm.

As can be seen from Fig. 5 the attenuation length strongly increases with the optical wavelength, reaching values of the order of a millimeter at $\lambda = 2.4$ mm. The thickness of

the film also strongly affects the SP losses. Figure 5(a) presents the angular dependences of the reflectivity, in the vicinity of the resonance for different thicknesses of the gold film for an optical wavelength 633 nm. For thin films the resonance becomes very broad, while for thick films the dip in the reflectivity reduces, which means that the coupling of light with the SP mode decreases.

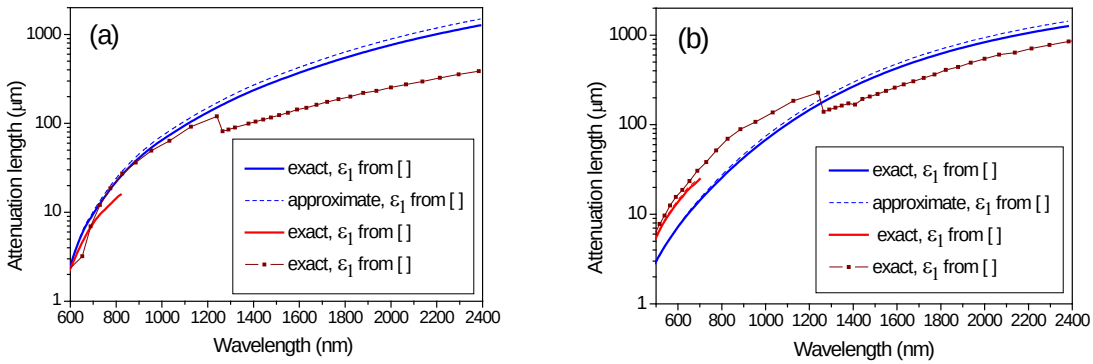

Fig. 5. Attenuation lengths for (a) gold and (b) silver, calculated for a broad spectral range with the exact (solid lines and solid lines with triangles) and approximate (dashed lines) models. The steps in the dependences, calculated with the data from Ref. [49], are due to the shifts present in this data.

The dependence of the attenuation length on the thickness of the gold film (see Fig.5(b)) shows that this length increases with the thickness of the film experiencing flattening of the dependence at larger thicknesses, which starts at around d=70 nm.

Figure 6 presents the angular dependences of the reflectivity, in the vicinity of the resonance for different thicknesses of the gold film for an optical wavelength 633 nm. For thin films the resonance becomes very broad, while for thick films the dip in the reflectivity reduces, which means that the coupling of light with the SP mode decreases.

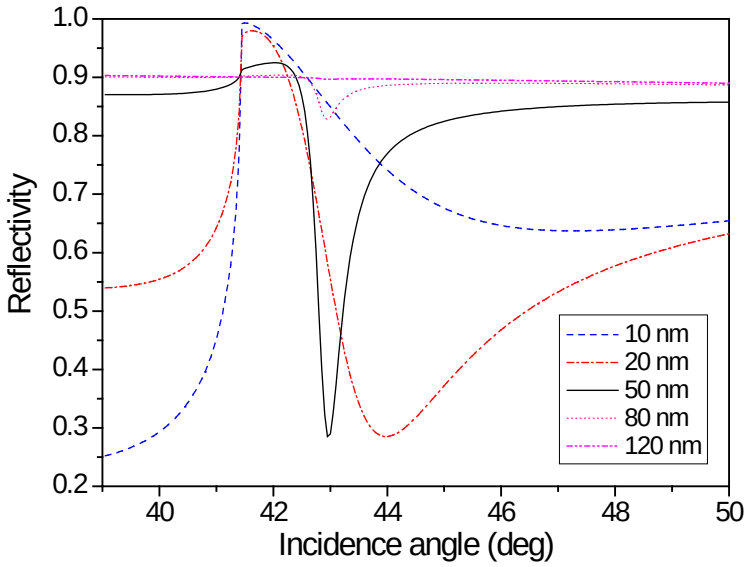

Fig. 6. The influence of the thickness of the gold film on the properties of SPs: SP resonance curves at 633 nm for different film thicknesses.

CHAPTER III

STUDY OF SURFACE PLASMON MODES IN METAL NANOSTRUCTURES WITH THE FAR FIELD SPECTROSCOPY

A. Investigated samples

We used two similarly produced grating structures, formed on evaporated 40 nm gold films deposited on glass substrates. The grating structure had a rectangular profile protruding approximately 25 nm above the film surface. Measurement of angle vs. wavelength of the diffracted light produced estimates of 705 (Sample1) and 760 nm (Sample 2) for the periods of the gratings. A sample of the SEM data for one of the structures is given in Fig. 7.

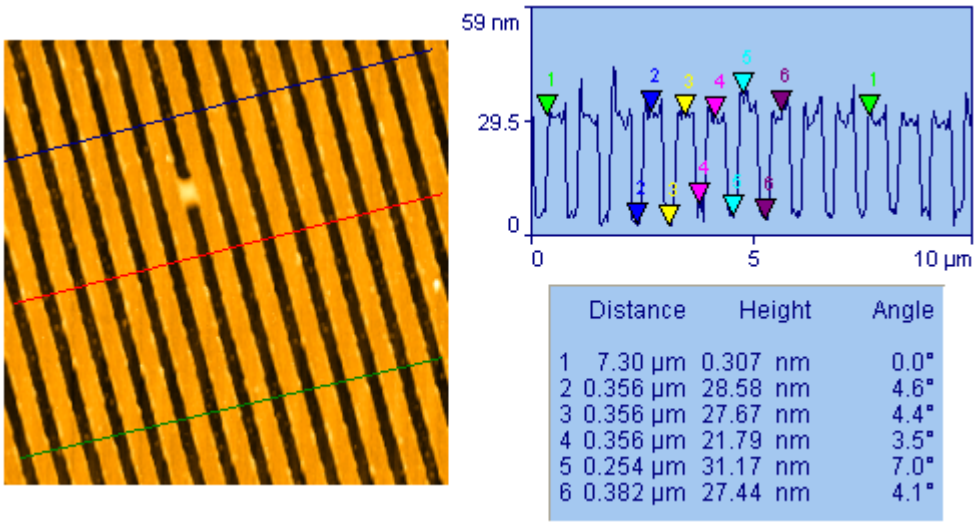

Fig. 7. A portion of the SEM data for Sample 2 (cross section and measurements from the blue line in the image).

B. Transmission for front-illuminated samples

The beam was incident directly on the grating and transmitted light was taken directly. The spectra for normalization of transmission data were taken by passing the laser beam through a portion of the gold film at some distance from the grating structure, so as to remove any absorption effects from the normalized data.

The spectra of light transmitted through the grating displayed two minima corresponding to +1 and -1 orders of the surface plasmon resonance excitation. The minimum corresponding to n=-1 order was more pronounced with efficiency of coupling of about 70%. The typical dependence of the transmitted light intensity on the wavelength is shown in Fig. 8. For example, for incidence angle of 4 degrees, the first resonance in the spectra around 728 nm corresponds to n=+1, and the second resonance at 832 nm corresponds to n=-1.

As incidence angle increases, the resonance corresponds to +1 order moves to shorter wavelength and the resonance corresponds to -1 order moves to longer wavelength. The data points were taken with incidence angle from -8 degrees to 8 degrees with a step of 1 deg. Close to normal incidence the step was reduced to a quarter of a degree. A gap between the resonance wavelengths of the two orders was observed in transmission at incidence angles around 0^0 as shown in Fig. 9.

Figure 10 shows the coupling efficiency between incidence light and two orders of surface plasmon modes. We define coupling efficiency using the following formula:

$$efficiency = (T_{\max} - T_{\min}) / T_{\max}$$

where T is the intensity of transmission near the resonance.

The coupling of the -1 order surface plasmon mode is much stronger than the +1 order mode. We can see abrupt changes of efficiency near the normal incidence, where the coupling of -1 order mode increases, the coupling of +1 order decreases close to 0.

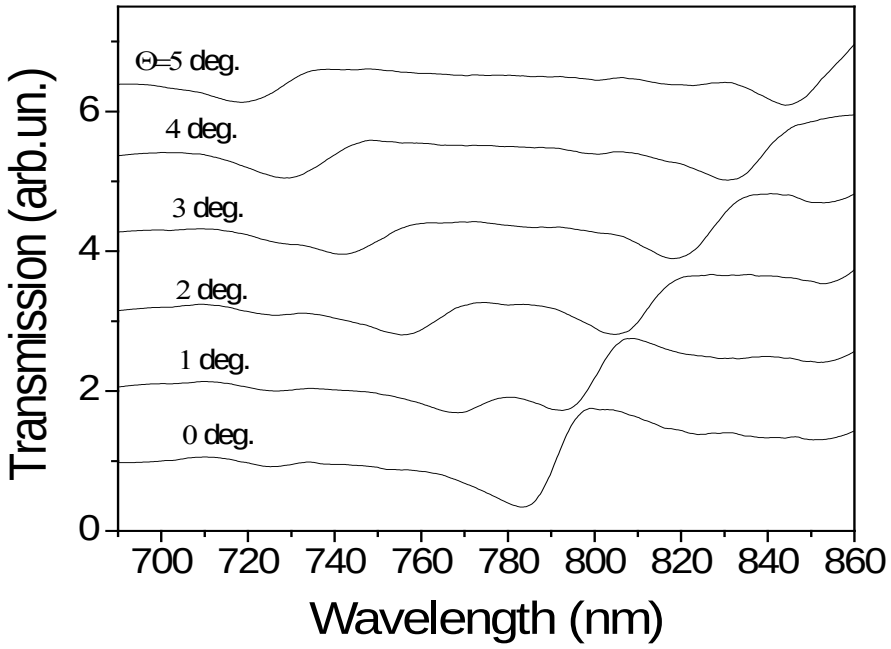

Fig. 8. Dependence of the normalized transmission on the wavelength versus incidence angles from 0 to 5 degrees. (Sample 2)

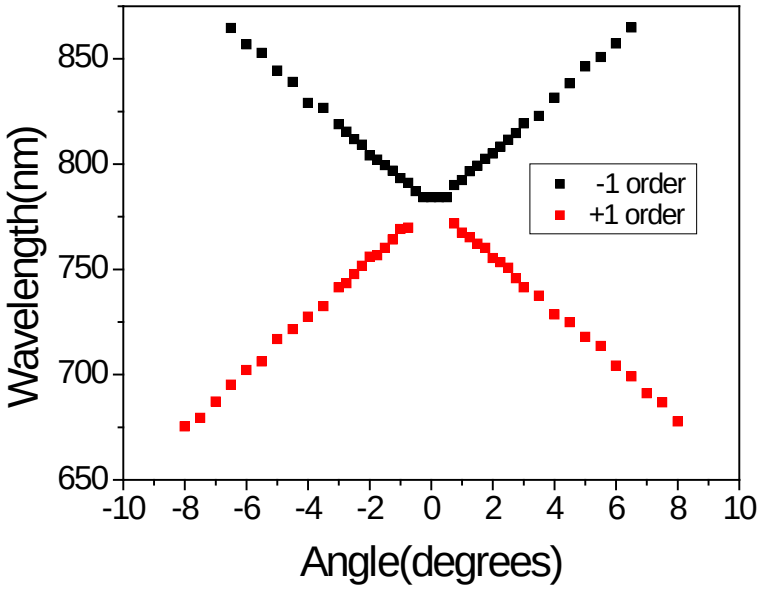

Fig. 9. Wavelength versus incidence angle for the transmission minimum. (Sample 2)

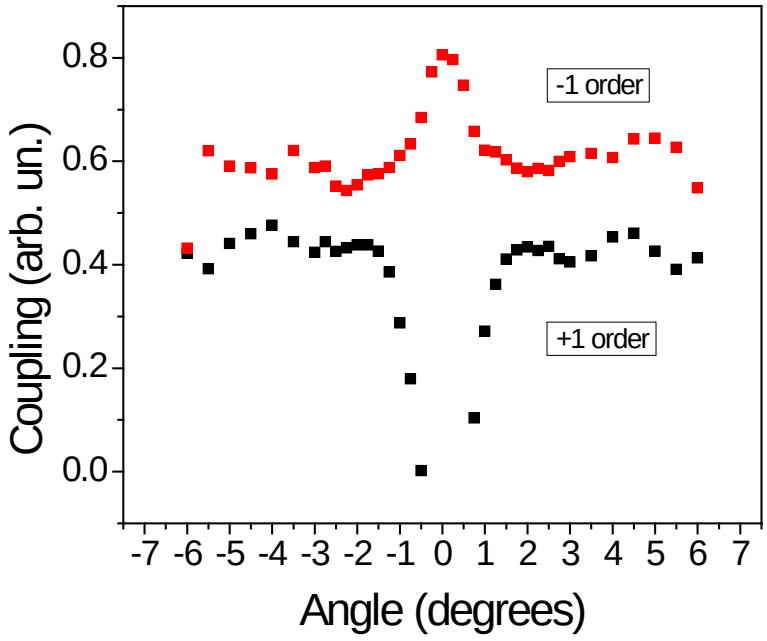

Fig. 10. Angular dependences of the coupling for the -1 order and +1 order SP modes in transmission. (Sample 2)

C. Transmission with back-illuminated samples

To compare the coupling to surface plasmons from different sides of the sample, we also studied the excitation when the sample was illuminated from the substrate side with the beam. The angular dependence of the resonance wavelengths is shown in Fig. 11. The resonance positions doesn't have significant shift from the case when the sample was front-illuminated. However, there is a noticeable difference in the coupling efficiency of the SP modes.

We investigated the back-illuminated case at the region of small incidence angle with smaller angular step. As is shown in Fig. 12, we see the presence of energy gap near the normal incidence angle.

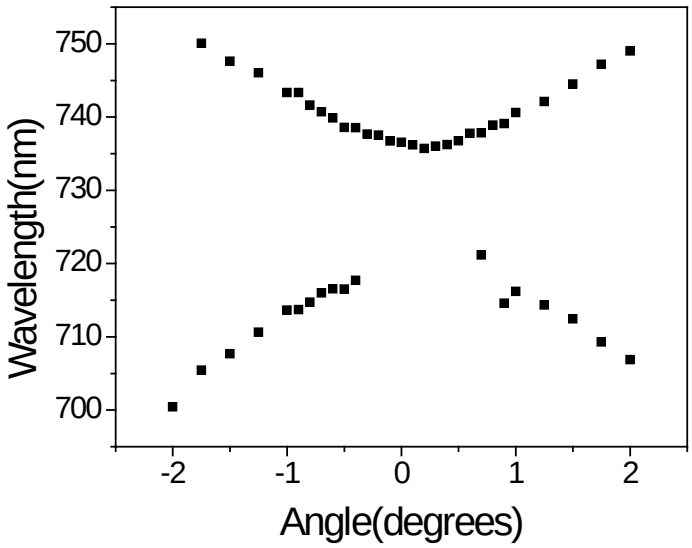

Fig. 11. Wavelength versus angle for minima in transmission from back illuminated sample (Sample 1).

Coupling efficiency of the incidence angle from -2 to +2 degrees from a back-illuminated sample was shown in Fig. 12. Compared to the case of front-illumination, coupling efficiency of +1 order SP mode stays near zero.

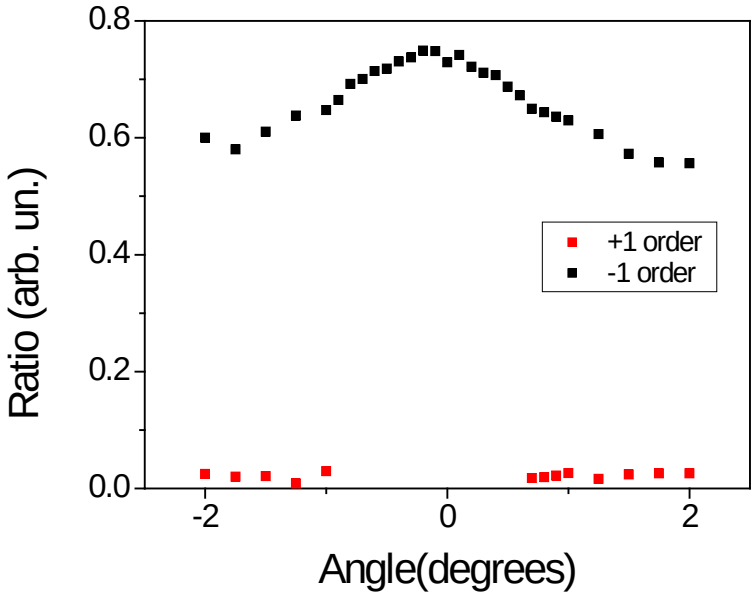

Fig. 12. Angular dependence of the coupling in transmission for back illuminated sample. (Sample 1)

D. Reflection with front illuminated samples

To measure the reflection, a beam splitter was placed in front of the sample to direct a portion of the reflected beam away from the polarizer toward the optical fiber. Spectra for normalization were taken from a specular reflection off a smooth portion of the film.

The spectra of light reflected from the gratings was shown in Fig. 13 at incidence angles from 0 to 3 degrees, the incidence angle wavelength dependence of resonance was

shown in Fig. 14. Compared to what we observed in the transmission spectra, the Fano type resonance seems to be inverted. For better comparison, we plotted the reflection and transmission spectra together in Fig. 15. We can see the difference in the coupling of SPs to reflected and transmitted light in both samples. It also suggested a slight shift of resonance wavelength at certain incidence angle.

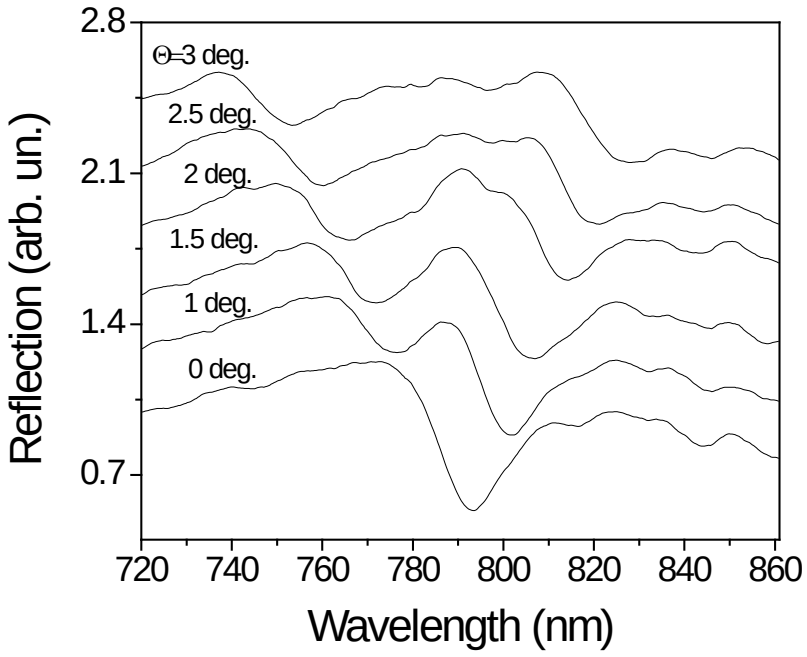

Fig.13. Dependence of the normalized reflection on the wavelength for incidence angles from 0 to 3 degrees. (Sample 2)

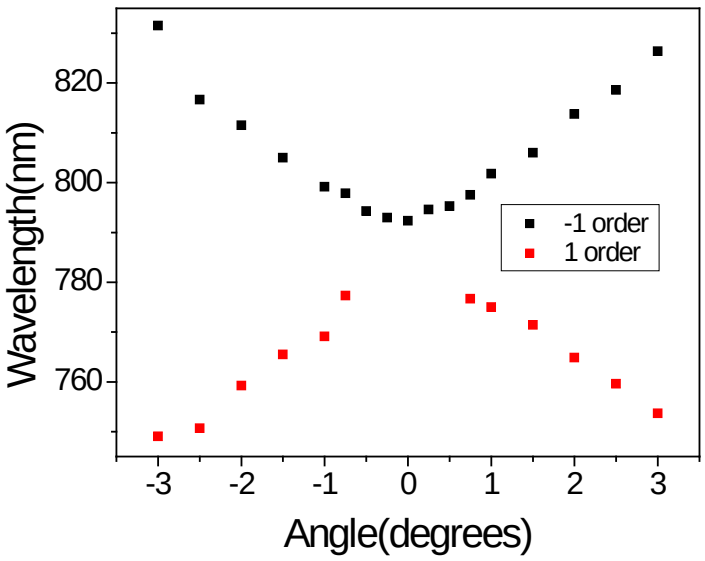

Fig. 14. Wavelength versus incidence angle for the reflection minimum (Sample2)

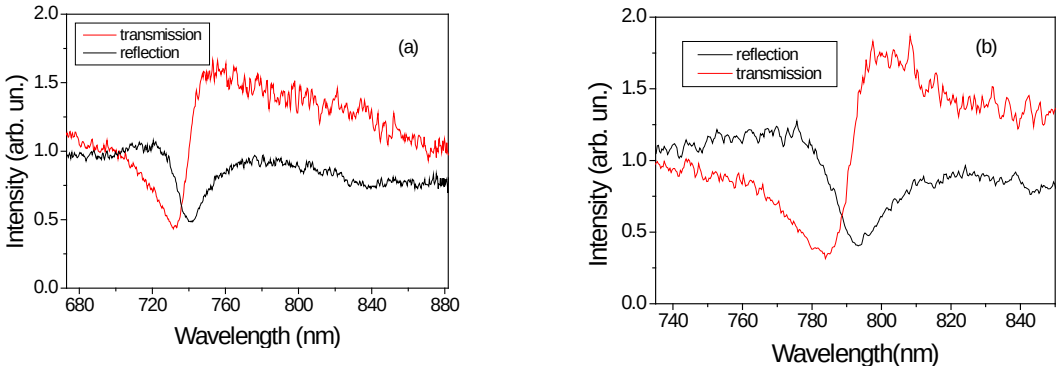

Fig. 15. Reflection and transmission spectra ((a) Sample 1, (b) Sample 2)

E. Reflection from back-illuminated samples

The spectra of the light reflected from a back-illuminated sample did not display any significant minima at expected resonance angles. Instead, these spectra displayed only

small-scale oscillations that appeared to result from interference between reflections from the glass and metal surfaces.

F. Diffraction

Diffracted light was collected with a spherical mirror focused on a paper diffuser to ensure all wavelengths in the spectrum were equally represented at the spectrometer. To check the change of the coupling for excitation from different sides of the sample, we measured diffracted light with back illumination.

A spectrum of diffraction at incidence angle of 2.5 degrees is presented in Fig. 16. The diffraction spectrum is cut off at 737 nm. This results from the diffracted light passing over the horizon. This cutoff follows the relation:

$$\lambda_{cutoff} = d(1+\sin\theta)$$

where θ is the angle between the incident light and the surface normal, with positive angles corresponding to incident and diffracted light on opposite sides of the normal. In our case, this limited us to observing only the +1 order SP resonance at angles of 1 degree or larger.

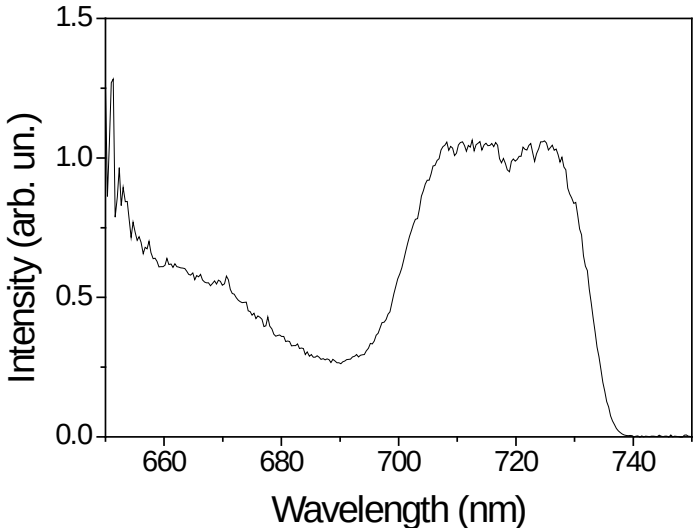

Fig.16. Diffraction spectra versus wavelength of a front illuminated sample at incidence angle of 2.5 degrees (Sample 1)

SP coupling at a grating surface is highly dependent on the polarization of the incident light. Maximum coupling is achieved when the magnetic field vector of the incident light is aligned along the rulings of the grating, or when the projection of the electric field vector onto the grating surface is perpendicular to the rulings. We measured SP coupling with light at normal incidence for varied polarizations. Normalized results for normal incidence are presented in Fig. 17. The data suggest a cosine squared dependence—i.e., only the component of the polarization perpendicular to the grooves contributes to SP coupling.

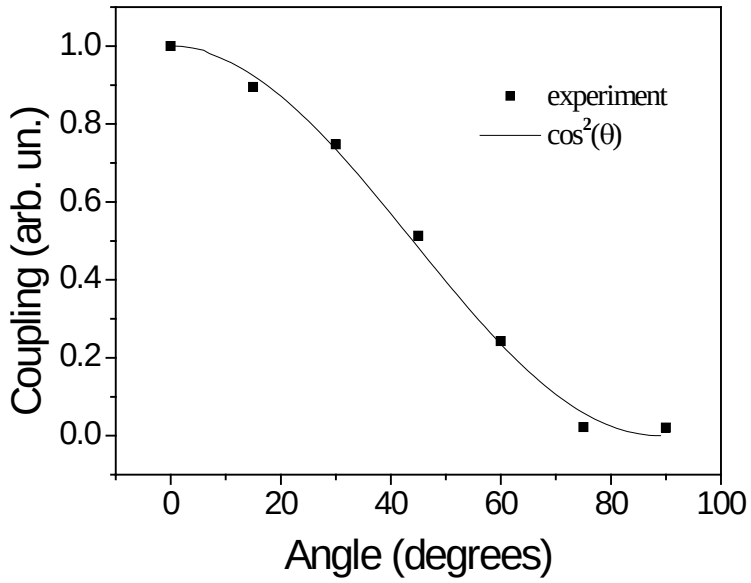

Fig. 17. Dependence of coupling on the polarization angle, with 0 degrees corresponding to polarization in the plane of incidence.

G. Reflection, transmission and diffraction in the interaction of light with a grating

The calculation for reflection and transmission coefficient is based on Botten's model [33,34]. A three-layer model with vacuum, metal grating and substrate and p-polarized incidence light was considered. The vacuum, wire, slit (the empty spacing between the wires of the grating) and the substrate regions were denoted as D0, D1, D2, and D3 respectively. The magnetic field in regions D0 and D3 obeys the Helmholtz equations:

$(\nabla^2 + k_0^2)H = 0$ in D0

$(\nabla^2 + k_3^2)H = 0$ in D3

where $k_0 = \frac{2\pi}{\lambda}$ and $k_3 = k_0 r_3$ and λ is the incidence wavelength.

In D0, the magnetic field can be expressed as Rayleigh series [2,50]:

$$H(x,y) = \sum_{p=-\infty}^{\infty} [\exp(-i\chi_0(y-h/2))\delta_{p,0} + R_p \exp(i\chi_p(y-h/2))]e_p(x)$$

where

$$e_p(x) = \exp(i\alpha_p x)/\sqrt{d}$$

$$\alpha_p = \alpha_0 + 2\pi p/d$$

$$\alpha_0 = k_0 \sin\phi$$

$$\chi_0 = k_0 \cos\phi$$

$$\chi_p = \begin{cases} \sqrt{k_0^2 - \alpha_p^2} \ for & |\alpha_p| \le k_0 \\ i\sqrt{\alpha_p^2 - k_0^2} \ for & |\alpha_p| > k_0 \end{cases}$$

Similarly, in region D3 ,

$$H(x,y) = \sum_{p=-\infty}^{\infty} T_p \exp(-i\eta_p(y+h/2))e_p(x)$$

$$\eta_p = \sqrt{k_3^2 - \alpha_p^2}$$

In the grating region D1 and D2, the field can be expressed as eigenfunction series, which came from the solution of the Helmholtz equation:

$$H(x,y) = \sum_n (a_n \sin(\mu_n y) + b_n \cos(\mu_n y))u_n(x)$$

where $u_n(x)$ is the eigenfunction of the slit region with the eigen value determined form the transcendental equation:

$$\cos(\beta c)\cos(\gamma g) - \frac{1}{2}\left(\frac{r_2^2}{r_1^2}\frac{\beta}{\gamma} + \frac{r_1^2}{r_2^2}\frac{\gamma}{\beta}\right)\sin(\beta c)\sin(\gamma g) = \cos(\alpha_0 d)$$

where β is the eigenvalue and $\gamma^2 = \beta^2 + \zeta^2$, $\zeta^2 = k_2^2 - k_1^2$, $\mu^2 = k_1^2 - \beta^2$

The boundary conditions at $y = \pm h/2$ imply that H is continuous at both boundaries and its derivative is continuous, by solving the four equations we get from the boundary condition the reflection and transmission coefficients, R and T:

$$R = F - i\chi^{-1} J(D_1 a^* + D_2 b^*)$$

where F is a vector whose entries are $F_p = \delta_{p0}$

$$\chi = diag(\chi_p / k_0^2)$$

$$D_1 = diag(D_{1m})$$

$$D_2 = diag(D_{2m})$$

$$T = i\eta^{-1} J(D_1 a^* - D_2 b^*)$$

where $\eta = diag(\eta_p / k_3^2)$, and a^* and b^* are the coefficients of amplitude:

$$\begin{bmatrix} I + iK^H \chi^{-1} JD_1 & I + iK^H \chi^{-1} JD_2 \\ -(I + iK^H \eta^{-1} JD_1) & I + iK^H \eta^{-1} JD_2 \end{bmatrix} = 2\begin{bmatrix} K^H F \\ 0 \end{bmatrix}$$

where $K_{pn} = \int_0^d \frac{1}{\bar{k}^2(x)} \bar{e}_p(x) u_n^+(x) dx$

$$J_{qm} = \int_0^d \frac{1}{k^2(x)} \bar{e}_q(x) u_m(x) dx$$

The infinite matrix for a^* and b^* can be truncated and solved numerically.

The calculation of transmission coefficient we obtained with Lockbihler's simplification [35]:

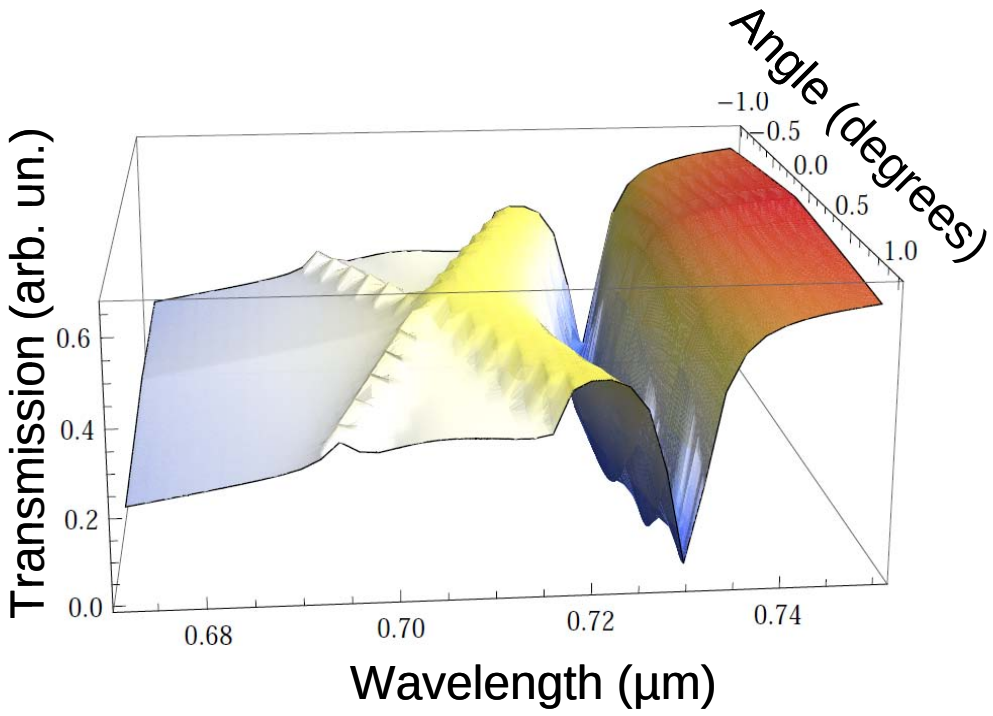

Fig. 18. Calculation of transmission spectra for wavelength versus incidence angle from -1 to 1 degrees: period=705 nm, wire width=350 nm

The calculation was performed with a grating of period 705 nm, and wire width 390 nm. The height of the grating is 50 nm. As we can see from the figures, the separation of the two resonances increases as we increase the incidence angle, which is what we observed in the experiment as well.

CHAPTER IV

BAND GAPS OF SP MODES IN METAL NANOSTRUCTURES

A. Previous studies

Excited SPs exhibit gaps in the energy spectrum (ω-gaps) [6,21,22,28], rendering these structures as simple plasmonic crystals. The gaps appear due to mode interaction near the crossing of their unperturbed dispersion curves and can be employed for wave guiding [37], developing sensors [51] and photonic notch filters [52]. The existence of momentum gaps (or k-gaps) was also proposed and confirmed in experimental [28] and theoretical works [53-55]. However, it has also been suggested that a k-gap is an artifact, resulting from the mode over-damping [56].

B. Experimental investigation of laser light interaction with gold nanostructures

We studied two types of metallic structures: a periodic array of gold nanowires on a glass substrate and a similar array with an additional gold sub-layer [57]. The periods of the arrays were chosen to provide SP resonances at the normal incidence close to the middle of the spectral range (from 650 to 850 nm) of the laser pulses. The configurations of the two samples produced by thermal vapor deposition and electron beam lithography are shown in Fig. 19(a). Both samples had a gold grating structure with rectangular profile. For the first sample the grating was thinner, and it was deposited onto an underlying gold film. The thickness of the films during the deposition was monitored with a quartz crystal monitor.

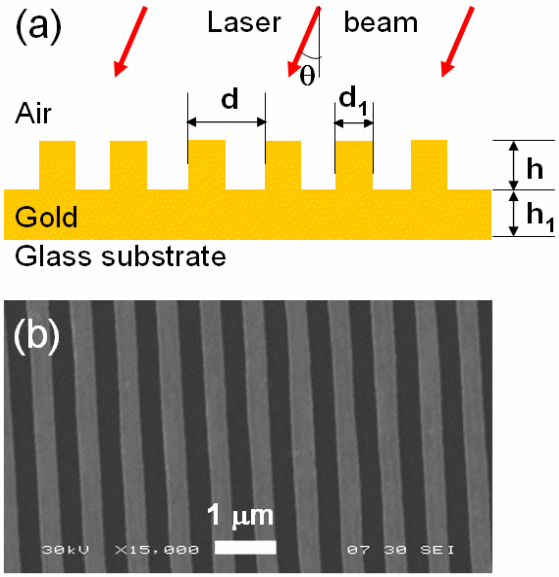

Fig. 19. Measured samples: (a). Schematic of the sample profile and the geometry of the laser beam incidence (red arrows). The two samples had the following dimensions. Sample 1A: $d = 705\,\text{nm}$, $d_1 = 390\,\text{nm}$, $h = 27\,\text{nm}$, $h_1 = 35\,\text{nm}$. Sample 2A: $d = 710\,\text{nm}$, $d_1 = 365\,\text{nm}$, $h = 50\,\text{nm}$, $h_1 = 0$. (b). SEM image of sample 2A.

Measurements of the transmitted light for a set of incidence angles were performed. A portion of the beam from a broadband pulsed laser (Rainbow, Femtolasers) was weakly focused and front-illuminated the sample. The sample was mounted on a rotation stage allowing for variation of the incidence angle from -6° to +6° with small steps and accuracy better than 0.05°. The light that interacted with the grating on the sample was selected by a small aperture and directed into an Ocean Optics spectrometer, registering the distribution of the spectral intensity. Normalized transmission spectra for two samples are shown as density plots in Fig. 20(a,c). The intensity distribution over incidence angle and wavelength displays two diagonal valleys corresponding to n=±1 orders of the SP resonance excitation, producing a decrease in the transmitted intensity.

The higher frequency branch demonstrates a narrowing for sample 1A and a slight broadening for sample 2A, when approaching the crossing region. This can be seen by comparing the shorter-wavelength dips of the spectral intensity profiles shown for a set of angles in Fig. 20(b,d), which exhibit asymmetric Fano-type resonances [58]. Such changes indicate damping variations of the SP modes. In particular, radiative damping can change due to a shift of the mode intensity distribution relative to the grooves of the grating, as the wavelength changes [12], and also the effect of the mode interaction due to Bragg scattering increases closer to the normal incidence, corresponding in k_{sp}-space to the boundary of the Brillouin zone [36].

The plots of the minima of the experimentally measured transmission show qualitatively different patterns of the dispersion relations for samples 1A,2A, depicted in Fig. 21(a,d). For sample 1A an ω-gap of about 30 meV is observed (Fig. 21(a)), which appears as a result of the interaction of $n = \pm 1$ modes and is mainly due to the presence of the second harmonic in the spatial profile of the nano-structure [56,59]. The lower and higher frequency branches can be related to the symmetric and antisymmetric modes [12,56,60]. The edges of the gap at $\theta = 0^o$ have wavelength values $\lambda_{h.f.} = 723\,\text{nm}$ and $\lambda_{l.f.} = 736\,\text{nm}$ and two different SP phase velocities $v_{sp,h.f.}$ and $v_{sp,l.f.}$ of the high and low

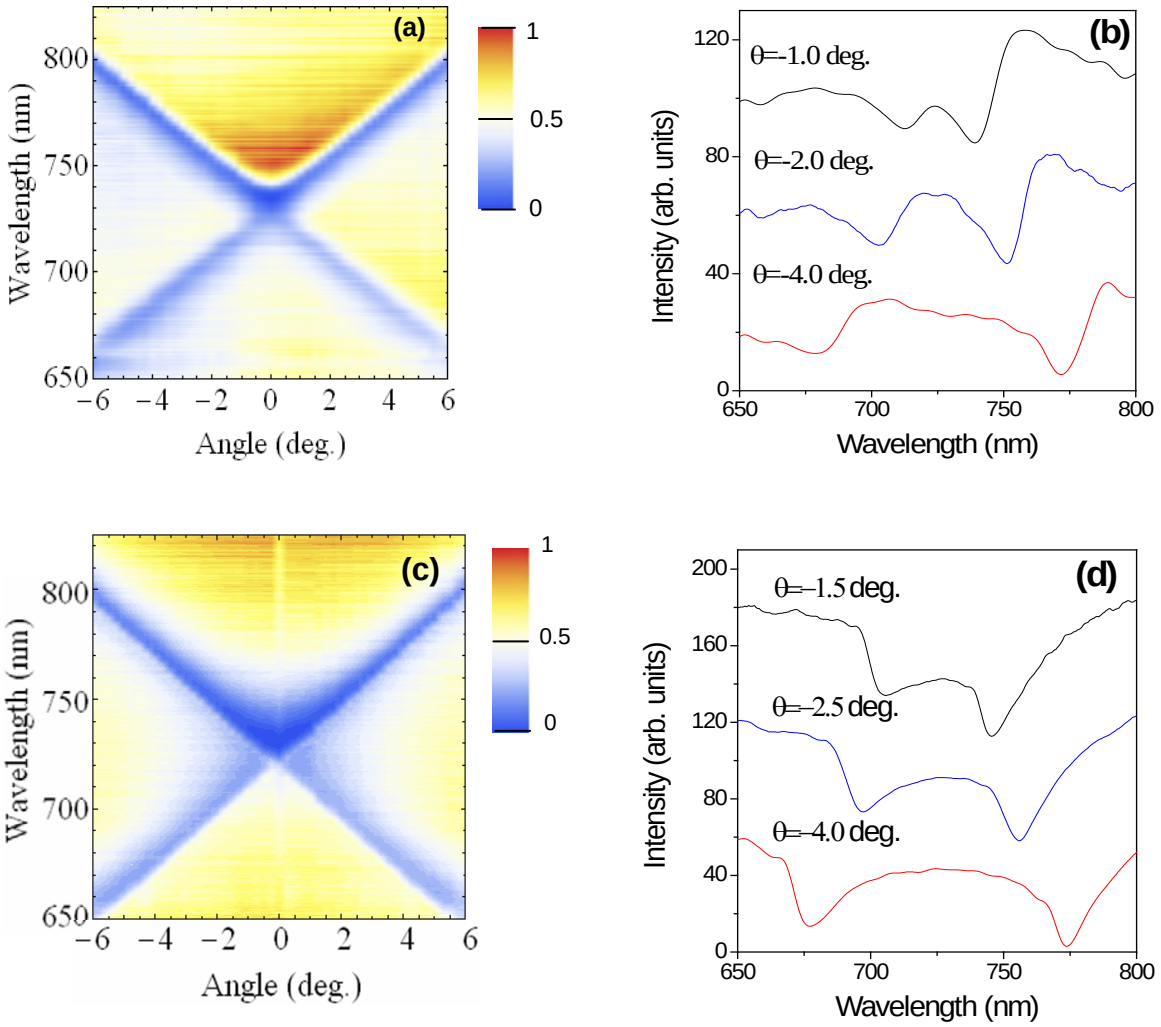

Fig. 20. Transmitted light intensity for different incidence angles and wavelengths: (a,b) sample 1A, (c,d) sample 2A. Fig.s (a, c) show false color density plots with the dark (blue) color corresponding to the reduction of the light transmission due to the SP excitation. Fig.s (b,d) depict the wavelength dependences of the intensity for a set of angles, showing that while in (b) the minimum at shorter wavelength becomes narrower for smaller angles, in (d) the similar minimum becomes slightly broader; in (b,d) the curves for different wavelengths are equidistantly shifted vertically for better viewing.

frequency SP modes, which have the following ratios to the speed of light c in air, $v_{sp,h.f.}/c = d/\lambda_{h.f.} = 0.968$ and $v_{sp,l.f.}/c = d/\lambda_{l.f.} = 0.951$, inferred from Eq. (1) for normal incidence.

For sample 2A, the mode pattern in the band-gap region is qualitatively different for higher and lower frequency branches. For the higher frequency branch, the dispersion curves with $n = \pm 1$ do not tend to merge when they approach the avoided crossing region, but rather form a gap in θ values (k-gap, $\Delta k = 1.91 \times 10^3$ cm^{-1}). The origin of such a gap cannot be attributed to a partial overlap of the approaching modes in the avoided crossing region, as was suggested [56], since only *one*, namely the lower frequency branch passes the center of this region.

Figs. 21(b,e) show the evolution of the transmission angular dependence for the two samples in the avoided crossing regions, indicated by dashed boxes in Fig. 21(a,d), as the wavelength is changed in small steps. With increasing wavelength the two side minima in the angular intensity distribution (Fig. 21(b), sample 1A), which are seen clearly for $\lambda = 716$ nm, initially merge into a valley and then re-appear again. In Fig. 21(e) (sample 2A) with increasing wavelength the two side minima stay separated until they disappear (four lower curves), and then two shallow minima are formed.

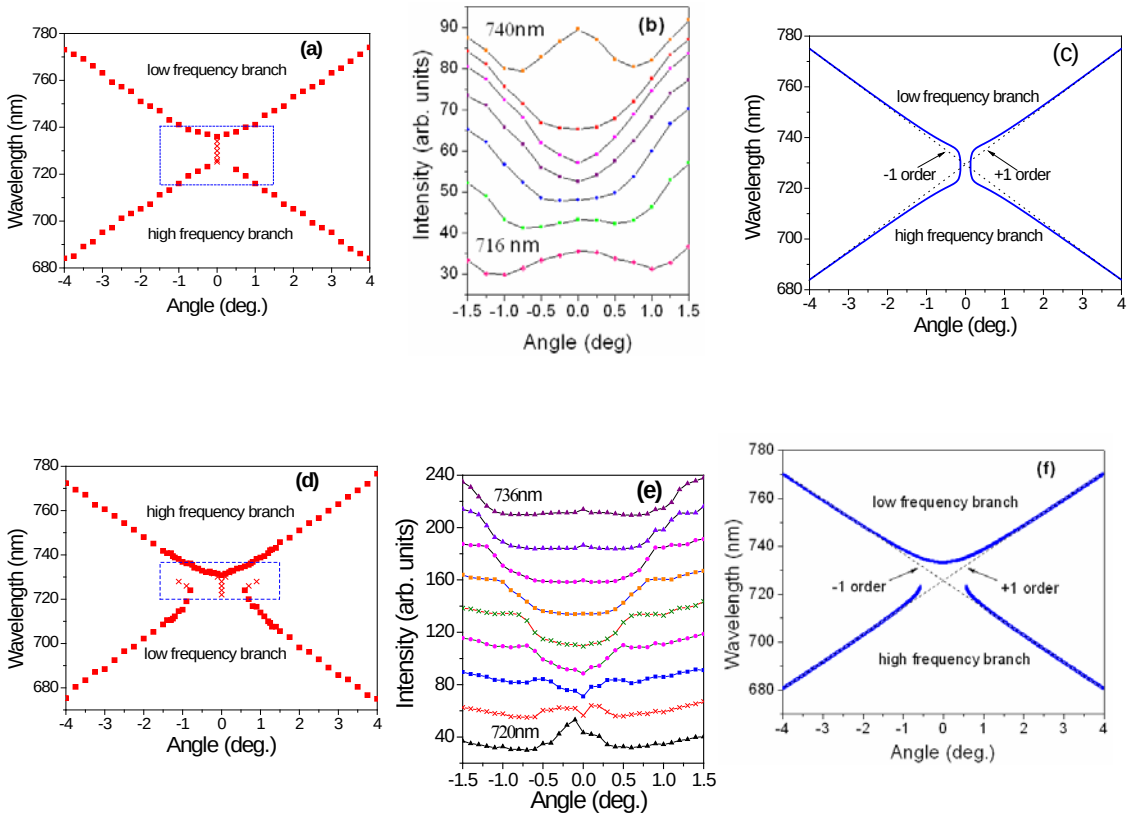

Fig. 21. Observed and calculated SP modes in the avoided crossing region: (a, d) minima of the transmission from the experiment, (b,e) transmitted intensity vs. angle for a set of wavelengths and (c,f) calculation of the SP modes of $n = \pm 1$ orders taking into account their interaction (Eq. (3), details in the text). Crosses in (a,d) show the extension of the observed minima into the gap region. Dotted lines in (c,f) show the dispersion dependences of the SP modes without interaction. Transmission dependences in the band-gap regions, indicated by dashed boxes in (a,d) are plotted for different wavelengths with steps of 4 nm in (b) and with steps of 2 nm in (e) for samples 1A and 2A, respectively.

C. Interpretation of avoided crossing and spectral gaps with coupled-mode theory

The following derivation follows general concepts of the coupled mode theory [61,62].

We consider two parallel waveguides a and b, the total field solutions can be written as linear combinations of the individual waveguide modes:

$$E(x,y,z) = a(z)E^{(a)}(x,y) + b(z)E^{(b)}(x,y)$$

$$H(x,y,z) = a(z)H^{(a)}(x,y) + b(z)H^{(b)}(x,y)$$

Consider two coupled SP modes with complex amplitudes $A_1(z)$ (mode with n=+1) and $A_2(z)$ (n=-1), counter-propagating along the z-axis and coupled with coefficients $K_{1,2}$ and $K_{2,1}$:

$$\frac{d}{dz}A_1(z) = ik_{sp;1}A_1(z) + iK_{2,1}A_2(z), \frac{d}{dz}A_2(z) = iK_{1,2}A_1(z) + ik_{sp;2}A_2(z),$$

where $k_{sp;1}$ and $k_{sp;2}$ are wave numbers of the two SP modes without interaction, corresponding to the incident light frequency $\omega = 2\pi c/\lambda$. The main mechanism of the interaction of these modes is their Bragg scattering with $2k_{gr}$ [21,36,56]. Assuming dependences $\propto \exp(ik_{sp}z)$, we find wave numbers as functions of ω taking into account the coupling of the modes:

$$k'_{sp;1,2} = (k_{sp;1} + k_{sp;2})/2 \pm q,\ q = \sqrt{\Delta^2 + G},\ \Delta = (k_{sp;1} - k_{sp;2})/2,\ \ G = K_{1,2}K_{2,1}. \qquad (30)$$

These equations show that if the condition $G < -\Delta^2$ is fulfilled, which corresponds to an interval of ω values, parameter q becomes imaginary, giving rise to a strong suppression (attenuation) of the SP modes (for small losses of the SP modes, as the first approximation, $k_{sp;1}, k_{sp;2}$ can be assumed to be real). Thus, for $G < -\Delta^2$ the two SP modes form an ω-gap (conservative coupling), while for $G > -\Delta^2$ the gap appears in the k'_{sp} values (dissipative coupling) [62]. When attenuation of the SP modes takes place or

the coupling constants are complex, the values of $k'_{sp;1,2}$ also become complex, so that the real parts $\mathrm{Re}\left[k'_{sp;1,2}\right]$ determine the phase constants of the modes, and the imaginary parts $\mathrm{Im}\left[k'_{sp;1,2}\right]$ determine their attenuation or amplification depending on the sign.

D. Calculation of the dispersion relations of SPs modes and comparisons to experiment

The theoretical approach for calculation of unperturbed dispersion curves is based on calculating the properties of a three-layer system consisting of glass, metal film, and air, with a grating present at the film-air interface. For certain incidence angles, light wavelengths, and grating parameters, the coupling of light and the surface plasmon mode can take place.

The results of the dispersion relation calculations with the model of two coupled SP modes (Eq. 3) are shown in Figs. 21(c,f) as $\lambda(\theta)$ dependences to enable direct comparison with the experimental data. The unperturbed dispersion relations $k_{sp;1}(\omega)$ and $k_{sp;2}(\omega)$ were calculated using the three layer model [41], taking into account the grating as an additional gold layer with effective thickness $h^{(1)}_{eff,1} = 15$ nm and $h^{(2)}_{eff,1} = 35\,\mathrm{nm}$ for samples 1A and 2A, respectively. For sample 1A, agreement with the experiment is obtained when the value of G has a negative real part and a relatively small imaginary part, so that in the assumption $\left|K_{1,2}\right| = \left|K_{2,1}\right|$ we obtain for contra-

directional waves $K_{1,2} = -K_{21} = (18 + 3.8i)$ meV. When the real part of G is positive and exceeds certain value, two almost vertical portions of the dispersion curves appear with a gap for the θ (or k) values. If this k-gap is small and damping is present, as in our case, these portions merge, forming a vertical line of minima in the transmission, as observed in the experiment (Fig. 21(a), the data points shown by crosses).

For sample 2A, the lower frequency branch looks similar to that of sample 1A. However, the higher frequency branch shows the divergence of the dispersion curves for n=+1 and n=-1 in the vicinity of the avoided crossing region ($\lambda < \lambda_c = 728$ nm), while in the region $\lambda > \lambda_c$ the portions of the dispersion curve tend to merge as the wavelength is approaching the center of the gap λ_c. The different behavior in these two wavelength regions provides evidence that the sign of the real part of the product G changes, as the wavelength changes from $\lambda < \lambda_c$ to $\lambda > \lambda_c$. The solid lines in Fig. 21(f) are calculated with $K_{12} = -K_{21} = 17\,i$ meV for $\lambda < \lambda_c$ and with $K_{12} = -K_{21}$=24 meV for $\lambda > \lambda_c$ and give good agreement with experimental points.

The change of the coupling constant can be related to a spatial shift of the intensity distribution relative to the grating slits with increasing wavelength, as the excitation switches from the higher frequency dark mode to the lower frequency bright mode, which was recently observed in a grating structure [12]. The coupled mode model *directly calculates dispersion dependences of the modes*, and thus, plots of Fig. 21(c,f)

suggest the possible existence of k-gaps. The experiment shows the presence of the transmission minima also in the gap region (in Fig. 21(d) these points are shown by crosses), which are not reproduced by the presented theory. These minima gradually disappear farther from the respective dispersion branch, which indicates their transitional nature.

CHAPTER V

SUMMARY AND CONCLUSIONS

In this thesis a study of the interaction of light with a metal grating is considered. By investigating transmission, reflection and diffraction of light a role of SPs in this interaction is elucidated. A derivation of the dispersion equation of SPs is presented. It is shown that the propagation length of SPs increases with the wavelength, and surface roughness leads to a reduction of this length. The interaction of light with gold nanostructures is experimentally studied. The distributions of the transmitted and reflected light versus incidence angle and wavelength clearly show efficient excitation of SP modes. They also give an evidence of the energy and momentum gaps in the SP spectrum. To describe interaction of light with metal nano-gratings we followed Rayleigh's approach. The formation of spectral gaps was explained in terms of the coupled-mode model.

REFERENCES

1. R. W. Wood, Phil. Mag. **4**, 396 (1902).

2. Lord Rayleigh (J. W. Strutt), Proc. R. Soc. London Ser. A **79**, 399 (1907).

3. U. Fano, J. Opt. Soc. Am. **31**, 213 (1941).

4. von A. Sommerfeld, Annalen der Physik. **28**, 4 (1909).

5. J. Zenneck, Annelen der Physik. **328**, 10 (1907).

6. R. H. Ritchie, E. T. Arakawa, J. J. Cowan, R. N. Hamm, Phys. Rev. Lett. **21**, 22 (1968).

7. H. Raether, Opt. Commun. **42**, 4 (1982).

8. A. Christ, S. G. Tikhodeev, N. A. Gippius, J. Kuhl, H. Giessen, Phys. Rev. Lett. **91**, 183901 (2003).

9. T. A. Leskova, A. A. Maradudin, W. Zierau, Opt. Commun. **249**, 23 (2005).

10. N. Mayani, F. Varnier, G. Rasigni, J. Opt. Soc. Am. A **7**, 2 (1990).

11. A. Karabutov, M. Sogoyan, Infrared Phys. Technol. **36**, 191 (1995).

12. C. Ropers, D. J. Park, G. Stibenz, G. Steinmeyer, J. Kim, D. S. Kim, C. Lienau, Phys. Rev. Lett. **94**, 113901 (2005).

13. H. Raether and E. Kretschmann, Z. Naturforsch. **23a**, 2135–2136 (1968).

14. U. Jönsson, L. Fägerstam, B. Ivarsson, B. Johnsson, R. Karlsson, Biotechniques **11**, 620 (1991).

15. A. A. Kolomenskii, P. D. Gershon, and H. A. Schuessler, Appl. Opt. **36**, 6539 (1997).

16. C. E. Jordan, A. G. Frutos, A. J. Thiel, and R. M. Corn, Anal. Chem. **69**, 4939 (1997).

17. A. V. Zayats, I. I. Smolyaninov, A. A. Maradudin, "Nano-optics of surface plasmon polaritons." Phys. Rep. **408**, 131 (2005).

18. A. Degiron, D. R. Smith, Opt. Express **14**, 4 (2006)

19. U. Fano, JOSA **31**, 213-221 (1941).

20. C. Skigin and R. A. Depine, Phys. Rev. E **59**, 3661 (1999).

21. M. Weber and D. L. Mills, Phys. Rev. B **27**, 2698 (1983).

22. W. L. Barnes, A. Dereux, T. W. Ebbesen, Nature **424**, 14 (2003).

23. J. B. Pendry, L. Martin-Moreno, F. J. Garcia-Vidal," SCIENCE **305**, 6 (2004).

24. T.J. Davis *et al*., Opt. Commun. **267**, 253 (2006).

25. Z. Chen, I. R. Hooper, J. R. Sambles, Phys. Rev. B **77**, 161405 (2008).

26. T. W. Ebbesen, H. J. Lezec, H. F. Ghaemi, T. Thio, P. A. Wolff, Nature **391**, (1998).

27. Q. Cao, P. Lalanne, Phys. Rev. Lett. **88**, 5 (2002).

28. D. Heitmann *et al*., Phys. Rev. B **35**, 2660 (1987).

29. W. L. Barnes, T. W. Preist, S. C. Kitson, J. R. Samples, Phys. Rev. B **54**, 9 (1996).

30. D. M. Whittaker, I.S. Culshaw, Phys. Rev. B. **60**, 2610-2618 (1999)

31. S. G. Tikhodeev, A. L. Yablonskii, E. A. Muljarov, N. A. Gippius, Teruya Ishihara, Phys. Rev. B **66**, 045102 (2002).

32. Kane Yee, IEEE **14**, 201 (1966).

33. L. C. Botten, M. S. Craig, R. C. McPhedran, Opt. Act. **28**, 8, 1103 (1981).

34. L. C. Botten, M. S. Craig, R. C. McPhedran, J. L. Adams, J. R. Andrewartha, Opt. Act. **28**, 3, 413 (1981).

35. H. Lochbihler, Phys. Rev. B **50**, 7 (1994).

36. E. Altewischer, X. Ma, M. P. van Exter, J. P. Woerdman, New J. Physics **8**, 57 (2006)

37. S. I. Bozhevolnyi, Phys. Rev. Lett. **86**, 3008 (2001)

38. A. Christ, T. Zentgraf, S. G. Tikhodeev, N. A. Gippius, O. J. F. Martin, J. Kuhl, Phys. Stat. Sol. **243**, 10 (2006)

39. P. Vasa, R. Pomraenke, S. Schwieger, Yu. I. Mazur, Vas. Kunets, Phys. Rev. Lett. **101**, 116801 (2008)

40. A. Kolomenski, A. Kolomenskii, J. Noel, S. Peng, H. Schuessler, Applied Optics, **48**, 5683-5691 (2009)

41. E. Kretschmann, Z. Phys. **241**, 313 (1971).

42. E. Kretschmann, Opt. Commun. **5**, 331 (1972).

43. E. Kröger and E. Kretschmann, Phys. Stat. Sol. (B) **76**, 515 (1976).

44. F. Toigo, A. Marvin, V. Celli and N. R. Hill, Phys. Rev. B, **15**, 5618 (1977).

45. S. O. Sari, D. K. Coben and K. D. Scherkoske, Phys. Rev. B **21**, 2162 (1980).

46. E. Fontana and R.H. Pantell, Phys. Rev. B **37**, 3164 (1988).

47. D. E. Gray, ed., *American Institute of Physics Handbook*, McGraw-Hill, New-York, 1972, p. 105.

48. U. Schröder, Surf. Sci. **102**, 118 (1981).

49. E.D. Palik, ed., *Handbook of Optical Constants of Solids*, (Academic, San Diego, 1985).

50. H. Lochbihler, J. Modern Optics **43**, 1867 (1996)

51. A. J. Benahmed and C.-M. Ho, Appl. Opt. **46**, 3369 (2007).

52. D. Noordegraaf, L. Scolari, J. Lagsgaard, T. T. Alkeskjold, G. Tartarini *et al.*, Opt. Lett. **33**, 986 (2008).

53. V. Celli, P. Tran, A. A. Maradudin and D. L. Mills, Phys. Rev. B **37**, 9089 (1988).

54. P.Halevi and O.Mata-Méndez, Phys. Rev. B **39**, 5694 (1989).

55. E. Popov, Surf. Sci. **222**, 517 (1989).

56. W. L. Barnes, T. W. Preist, S. C. Kitson, J. R. Samples, Phys. Rev. B **54**, 9 (1996).

57. Alexandre Kolomenskii, Siying Peng, Jeshurun Hembd, Andrei Kolomenski, John Noel, Winfried Teizer and Hans Schuessler, Dept. of Physics, Texas A&M University, in preparation

58. U. Fano, Phys. Rev. **124**, 1866-1878 (1961).

59. S.H. Zaidi, M. Yousaf and S. R. Brueck, J. Opt. Soc. Am. B **8**, 770 (1991); Ibidem, 1348 (1991).

60. J. W. Lee, T. H. Park, P. Nordlander and D. M. Mittleman, Phys. Rev. B **80**, 205417 (2009).

61. H. Kogelnik H. and C.V. Shank, J. Appl. Phys. **43**, 1972 (1972).

62. R. Spreeuw, R. C. Neelen, N. J. Druten, E. R. Eliel, J. P. Woerdman, Phys. Rev. A **42**, 4315 (1990).

APPENDIX A

DERIVATION OF BOUNDARY CONDITIONS

The boundary conditions (5-7) can be derived in the following way: For (6), we consider an integral of the magnetic field over a rectangular loop, encompassing a segment of the boundary.

$$\oint H = \int_{l1} H_1 dl_1 + \int_{l2} H_2 dl_2$$

where l1 and l2 are the sides of the rectangular loop parallel to the boundary corresponding to medium 1 and 2, and l1=-l2 and we took into account that the integral over the two sides perpendicular to the boundary goes to zero in the limit when the loop is squeezed to the surface. Then we apply Stokes's theorem to the left side the last equation, and use Eq. (1),

$$l_1(H_{1y} - H_{2y}) = \int \nabla \times H ds = \int ds \varepsilon_1 \frac{1}{c_i} \frac{\partial E_i}{\partial t} = \frac{\partial}{\partial t} \int_s (\frac{\varepsilon_i}{c_i} E_i) ds$$

Since the area of the rectangular loop goes to zero, we have the integral goes to zeros, which implies:

$$H_{1y} - H_{2y} = 0$$

Boundary condition (5) can be obtained in the same way.

To derive boundary condition (7), we have to consider equation (3) and integrate it over a rectangular volume containing a small part of the interface. We consider the electric field that goes through the surface, and since the field flux through the surface

perpendicular to the boundary goes to zero, we only have the electric field which goes through the surface parallel to the boundary:

$$\int_S \varepsilon E ds = \int_{S1} \varepsilon_1 E_1 ds + \int_{S2} E_2 ds$$

Since the two surfaces have the relation S1=-S2, by applying the Gauss's theorem we obtain:

$$S_1(\varepsilon_1 E_{1z} - \varepsilon_2 E_{2z}) = \int_V \nabla \cdot (\varepsilon E) dv = 0 \quad ,$$

the integral over the rectangular volume goes to zero in the limit, when the volume is squeezed to the surface, consequently

$$\varepsilon_1 E_{1z} - \varepsilon_2 E_{2z} = 0$$

which is Eq. (7).

APPENDIX B

DERIVATION OF THE DIELECTRIC CONSTANT OF A FREE ELECTRON GAS

Consider a simple model of electrons in a metal under action of oscillating electrical field $E = E_0 e^{i\omega t}$. The electrons move according to the Newton's second law:

$$m\frac{d}{dt}v = -eE .$$

Then we find the displacement amplitude of an electron:

$$x = \frac{1}{-\omega^2 m}(-eE_0) = \frac{eE_0}{\omega^2 m}$$

This displacement of electrons will induce polarization $P = -4\pi eNx$, where N is the number of electrons in a unit volume.

Then for the dielectric susceptibility we have:

$$\varepsilon = \frac{D}{E} = \frac{E+P}{E} = 1 - 4\pi eN\frac{eE_0}{m\omega^2}$$

which is Eq. (17)

Consequently, the obtain the dielectric function $\varepsilon = 1 - \frac{\omega_P^2}{\omega^2}$, where $\omega_P = \sqrt{4\pi eN\frac{e^2}{m}}$ is the so called plasmon frequency.

The derivation of the relation between the polarization and the displacement of charges can be carried out in the following way. In SGS system of units, Gauss's law provides:

$$\int_S Eds = 4\pi \sum_i q_i$$

Consider now a thin element of a medium perpendicular to the displacement x of the electrons. Then $\sigma = -eNx$ represents the surface density of charges. In some point A between the sides of the element due to this separation of charges we will have additional electric field which is just due to polarization. Since this field is uniform we can consider this similar to the field in a plane capacitor. Then,

$$P = \Delta E$$

$$\Delta E = \Delta E_{+\sigma} + \Delta E_{-\sigma}$$

$$\Delta E_{+\sigma} = \Delta E_{-\sigma}$$

$$2S\Delta E_{+\sigma} = 4\pi\sigma S$$

Thus, polarization is:

$$P = \Delta E = 4\pi\sigma = -4\pi eNx$$

CONTACT INFORMATION

Name:	Siying Peng
Professional Address:	Department of Physics Texas A&M University 4242 TAMU College Station, TX 77843
Email Address:	pengsy1988@gmail.com
Education:	B.S., Physics, Texas A&M University, May 2011 B.S., Mathematics, Texas A&M University, May 2011